**Atmospheric
Chemistry
and Physics
Discussions**

Presenting SAPUSS

M. Dall'Osto et al.

Presenting SAPUSS: solving aerosol problem by using synergistic strategies at Barcelona, Spain

M. Dall'Osto[1,2,3], X. Querol[1], A. Alastuey[1], M. C. Minguillon[1], M. Alier[1],
F. Amato[1], M. Brines[1], M. Cusak[1], J. O. Grimalt[1], A. Karanasiou[1], T. Moreno[1],
M. Pandolfi[1], J. Pey[1], C. Reche[1], A. Ripoll[1], R. Tauler[1], B. L. Van Drooge[1],
M. Viana[1], R. M. Harrison[2,16], J. Gietl[2], D. Beddows[2], W. Bloss[2], C. O'Dowd[3],
D. Ceburnis[3], G. Martucci[3], S. Ng[4], D. Worsnop[4], J. Wenger[5], E. Mc Gillcuddy[5],
J. Sudou[5], R. Healy[5], F. Lucarelli[6], S. Nava[6], J. L. Jimenez[7], F. Gomez Moreno[8],
B. Artinano[8], A. S. H. Prevot[9], L. Pfaffenberger[9], S. Frey[10], F. Wilsenack[11],
D. Casabona[12], P. Jiménez-Guerrero[13], D. Gross[14], and N. Cotz[15]

[1]IDAEA-CSIC, C/Jordi Girona 18–22, 08034 Barcelona, Spain
[2]National Centre for Atmospheric Science, Division of Environmental Health and Risk
Management, University of Birmingham, Birmingham, UK
[3]School of Physics, Centre for Climate and Air Pollution Studies, National University of Ireland
Galway, University Road, Galway, Ireland
[4]Center for Aerosol and Cloud Chemistry, Aerodyne Research, Inc., Billerica, MA, USA

Title Page

Abstract | Introduction

Conclusions | References

Tables | Figures

◄◄ | ►►

◄ | ►

Back | Close

Full Screen / Esc

Printer-friendly Version

Interactive Discussion

[5]Department of Chemistry and Environmental Research Institute, University College Cork, Ireland
[6]National Institute of Nuclear Physics (INFN) and Department of Physics and Astronomy, University of Florence, Sesto Fiorentino, Italy
[7]Dept. of Chemistry and Biochemistry, University of Colorado, Boulder, CO, USA
[8]CIEMAT, Environment Department, Av. Complutense 40, 28040 Madrid, Spain
[9]Paul Scherrer Institut, Laboratory of Atmospheric Chemistry, 5232 Villigen PSI, Switzerland
[10]Jenoptik, Defense and Civil Systems, Sensor Systems Business Unit, Teltow, Germany
[11]Wehrwissenschaftliches Institut für Schutztechnologien, Germany
[12]Area de Medi Ambient, Diputació de Barcelona, Spain
[13]Física de la Tierra, Universidad de Murcia, Murcia, Spain
[14]Department of Chemistry, Carleton College, MN, USA
[15]Gencat, Spain
[16]Department of Environmental Sciences/Center of Excellence in Environmental Studies, King Abdulaziz University, Jeddah, 21589, Saudi Arabia

Correspondence to: M. Dall'Osto (manuel.dallosto@gmail.com)

Title Page

Abstract | Introduction

Conclusions | References

Tables | Figures

◀ | ▶

◀ | ▶

Back | Close

Full Screen / Esc

Printer-friendly Version

Interactive Discussion

Abstract

This paper presents the summary of the key objectives, instrumentation and logistic details, goals, and initial scientific findings of the Marie Curie Action FP7-EU SAPUSS project carried out in the Western Mediterranean Basin (WMB) from 20 September–20 October 2010. The experiment involved concurrent measurements of aerosols with multiple techniques occurring simultaneously. The key objective is to deduce point aerosol source characteristics and to understand the atmospheric processes responsible for their generations and transformations. The unique approach is the large variety of instrumentation deployed simultaneously in six monitoring sites in Barcelona (NE Spain) and around the city, including: a main road traffic site, two urban background sites, a regional background site and two tower sites (150 m and 545 m a.s.l., 150 m and 80 m above ground, respectively). The SAPUSS experiment allows us to interpret the variability of aerosols levels and composition in an Urban Mediterranean, an environment not well characterized so far. During SAPUSS different air mass scenarios were encountered, including warm Saharan, cold Atlantic, wet European and stagnant Regional ones and presenting different local meteorology and boundary layer conditions. Analysis of part of the data collected allows us to compare the monitoring sites as well as to draw scientific conclusions about relevant air quality parameters. High levels of traffic-related gaseous pollutants were measured at the urban ground level monitoring sites, whereas layers of tropospheric ozone were recorded at tower levels. Particularly, tower level night time average ozone concentrations ($80 \pm 25 \, \mu g \, m^{-3}$) were up to double than ground level ones. Particle number concentrations ($N_{>5}$: $9980 \pm 6500 \, cm^{-1}$, average of all measurements) were generally traffic dependent, although a contribution from two different types of nucleation events was also found. Analysis of the particulate matter (PM) mass concentrations shows an enhancement of coarse particles ($PM_{2.5-10}$) at the urban ground level (+64 %, average $11.7 \, \mu g \, m^{-3}$) but of fine ones (PM_1) at urban tower level (+28 %, average $14.4 \, \mu g \, m^{-3}$). Preliminary modeling findings reveal an underestimation of the fine accumulation aerosols. In summary, this

paper lays the foundation of SAPUSS, an integrated study of relevance to many other similar urban Mediterranean coastal environment sites.

1 Introduction

Atmospheric particles have several adverse effects on human health (Pope and Dockery, 2006) and atmospheric visibility, and partly compensate climate forcing by greenhouse gases (IPCC, 2007). These effects depend on particle diameter and chemical composition, as well as on mass and number concentrations which exhibit large temporal and spatial variability. A major complexity associated with PM involves its measurement. Airborne particles come in sizes ranging over 5 orders of magnitude from 2 nm to larger than 100 µm, and contain thousands of chemical compounds. There are multiple aerosol sources, and emissions from the same source will change with time and operating conditions. In other words, since particles undergo a variety of physical and chemical transformations in the atmosphere, what is measured at the source may not be what will be found in the atmosphere. A detailed knowledge of the chemical composition of particles – alongside knowledge of their size and concentration – is important to apportion the sources of PM in the atmosphere.

There are two general approaches to making atmospheric measurements. The first one is remote sensing and the second is in-situ. In the former one, some atmospheric parameters of interest are derived indirectly by the changes in atmospheric radiation that result from the presence of the parameter. The remote sensing instrument detects changes in atmospheric thermal (infrared) and wave (visible, ultraviolet, microwave) radiation produced by the parameter. Examples include the LIDAR (Light Detection And Ranging) and the ceilometer, which are techniques that provides vertical profiles of the aerosol optical properties with a high vertical and temporal resolution. By contrast, the latter in-situ measurements involve the direct sampling of the atmosphere. A sample of the atmosphere (air) is brought into the instrument and is analyzed for its properties (McMurry, 2000). Whilst the technology to accurately count, size, and determine the

Presenting SAPUSS

M. Dall'Osto et al.

mass concentration of particles in real time is fairly well established, the chemical analysis of aerosol is not as easily performed. The most direct method is to collect particulate matter on a filter or impactor substrate over a period of hours and to analyze the material using standard analytical procedures. These so called off-line aerosol measurements carry many intrinsic limitations including: generally low temporal resolution, evaporation or loss of volatile components, reaction of chemically unstable compounds and interchange with the gas phase during sampling. In other words, off-line aerosol techniques do provide very valuable quantitative information on several chemical compounds, but the low time resolution of most of them often do not allow extracting any information on the formation and the evolution of processes happening in the atmosphere. However, in the last few years there has been considerable development of instrumentation capable of sizing and chemically characterizing airborne particles by using real time particle mass spectrometry techniques (so called on-line aerosol measurements). Whilst a number of research based real-time aerosol mass spectrometers not commercially available are currently used (Pratt and Prather, 2011a, b), at least two commercial instruments are now widely available: the Aerodyne Aerosol Mass Spectrometer (AMS) (Canagaratna et al., 2007) and the TSI Aerosol Time-of-Flight Mass Spectrometer (ATOFMS) (Gard et al., 1997). The ideal particle mass spectrometer should be able to determine the size of individual airborne particles, and to provide a quantitative measure of each of the molecular constituents in real time, but neither the AMS nor the ATOFMS reach the ideality. In summary, an array of instruments is required to get close to the full picture of the source identification and evolution (aging) of particles in the atmosphere.

The objective of this paper is to present SAPUSS, a Marie Curie Action (FP7-PEOPLE-2009-IEF-254773) which fundamentally aims to synergistically deploy a number of state-of-the-art aerosol measurements techniques which will result in significant advances in our knowledge of atmospheric aerosol properties. State of the art real time aerosol techniques have not been widely deployed in the WMB areas although it is worth to mention that recently the DAURE (Determination of the sources of

Presenting SAPUSS

M. Dall'Osto et al.

Title Page

Abstract | Introduction

Conclusions | References

Tables | Figures

◄ | ►

◄ | ►

Back | Close

Full Screen / Esc

Printer-friendly Version

Interactive Discussion

atmospheric Aerosols in Urban and Rural Environments in the Western Mediterranean) project was carried out in the same area (Minguillón et al., 2011; Mohr et al., 2012). The original SAPUSS proposal was extensively expanded due a large number of collaborators willing to take part (Table 1). SAPUSS generated a number of atmospheric chemistry and physics (ACP) highlights reported in the research manuscripts of this ACP special issue. This introductory paper aims to overview the sampling campaign which took part mainly in Barcelona (Spain) between 20 September and 20 October 2010 (local time, UCT + 2). Whilst all the SAPUSS scientific findings will be reviewed in a final summarizing manuscript, we feel the complexity of the SAPUSS field study (six monitoring sites) merit an introductory overview paper in order to present not only the project, but also the concentrations values of the EU regulated quality parameters monitored during SAPUSS.

The main SAPUSS scientific objectives were:

– To interpret the variability of aerosol levels and composition in the urban Mediterranean environment of Barcelona, the second largest city in Spain and the fifth largest metropolitan urban agglomerate of Europe.

– To study in detail the processes of formation and transformation of aerosols in the urban background and road site atmospheric environment.

– To elucidate the fate of freshly generated traffic particles at different altitudes within the urban boundary layer.

– To examine the spatial scales of urban nucleation events and variations in ultra-fine aerosol particle characteristics in locations with differing land use and emission profiles, to examine the meteorological context for nucleation events, to provide number concentrations and ultra-fine aerosol particle composition during nucleation events.

Presenting SAPUSS

M. Dall'Osto et al.

Title Page

Abstract	Introduction
Conclusions	References
Tables	Figures

◀◀   ▶▶

◀   ▶

Back   Close

Full Screen / Esc

Printer-friendly Version

Interactive Discussion

- To understand the physical and chemical differences of the urban aerosols detected at ground level (road and urban background sites) and above the city (2 towers) in three spatial dimensions.

- To determine spatial differences in aerosol particle size distributions and to interpret those differences in terms of the sources and physico-chemical transformations responsible simultaneously at the road, background, tower and regional background sites.

- To study the structure of the atmospheric boundary layer and the influence of boundary layer vertical structure upon air pollution processes, especially in the context of diurnal changes.

- To quantify the contribution of both exhaust and non-exhaust traffic generated particles in the road site relative to the urban background one.

- To apply receptor modelling to organic and inorganic species, as well as physical properties such as particle number and aerosol size distributions in order to obtain scientifically and environmentally relevant results to allow the identification of emission sources and their respective contributions to the PM mass in ambient air.

Our measurements approach involved (as summarized in Table 2):

- Simultaneous measurements of gaseous pollutants and local meteorological parameters.

- Simultaneous measurements of the vertical and horizontal aerosol profiles from two ceilometers positioned vertically and horizontally in the urban agglomerate of Barcelona.

- Simultaneous measurements of hourly PM_1, $PM_{2.5}$ and PM_{10} aerosol mass concentrations at six sites to study the vertical and horizontal aerosol mass distributions (six optical counters).

Presenting SAPUSS

M. Dall'Osto et al.

- Simultaneous measurements of size resolved particle number concentrations by deploying 4 Differential Mobility Analyser – DMA – and 11 Condensation Particle Counter – CPCs – (4 Scanning Mobility Particle Sizer – SMPS – and 7 single CPCs altogether).

- Simultaneous measurements of inorganic and organic components of the PM_1, $PM_{2.5}$ and PM_{10} aerosol mass loadings at different sites (10 high-volume samplers altogether).

- Simultaneous measurements of co-located highly time-resolved instruments (Black Carbon, ATOFMS, HR-ToF-AMS and streaker samples) in order to identify unique sources which would not be possible without multiple highly-resolved instruments working in concert. Two super sites are used (urban background and road site) where simultaneously non-refractory and refractory aerosol species at hourly concentrations are obtained, as well as single particle information in real time.

Additional advantages will be obtained when data from suites of instruments are further combined with atmospheric models. Among the receptor-oriented models, chemical mass balance (CMB), positive matrix factorization (PMF), principal component analysis (PCA) and multilinear engine (ME) are widely used to evaluate the effects of the source emissions. The joint on-line and off-line data generated from SAPUSS will be the input of the receptor-oriented models, which will help to re-construct the impacts of emissions from different sources of atmospheric pollutants such as PM. In particular the hourly data series for inorganic refractory constituents obtained with the streaker samples, those from co-located AMS-ATOFMS measurements, and BC, CPC and aerosols size distributions measurements will constitute a unique ground breaking basis for the application of source receptor modelling at hourly resolution scale.

2   Study area and monitoring sites

The SAPUSS campaign was carried out mainly in Barcelona, a city located in the WMB in the North East (NE) part of Spain. The Mediterranean region is often exposed to multiple stresses, such as a simultaneous water shortage and air pollution exposure (IPCC, 2007). The WMB possesses peculiar and complex atmospheric dynamics affecting regional, mesoscale and local meteorological processes including: (1) the influence of the Azores high-pressure system in the meteorology of the Iberian Peninsula (IP); (2) the coastal ranges surrounding the Mediterranean coast; (3) the influence of the Iberian and Saharan thermal lows causing weak pressure gradients over the Mediterranean; (4) the intense breeze action along the Mediterranean coast favoured by the prevailing low advective conditions; (5) the scarce summer precipitation; and (6) the intense seasonal contrast concerning temperature, humidity and rainfall (Millan et al., 1997; Soriano et al., 2001; Rodriguez et al., 2002, 2003; Jorba et al., 2004; Pereza et al., 2006). Furthermore, the WMB is affected by the transport of dust from North Africa which reaches the maximum frequency during summer contributing to the increase in the PM concentration in the region (Querol et al., 1998, 2009; Rodriguez et al., 2003). As a result, a number of comparative studies on the variability of PM levels and the composition along the WMB report high atmospheric aerosol loadings (e.g. Querol et al., 2001a, b, 2004; Viana et al., 2008; Kocak et al., 2008). It is worth to mention that East Mediterranean countries also show high levels of atmospheric PM compared to Northern and some Central European regions (Kanakidou et al., 2011).

Within the WMB, Barcelona is confined in a coastal region characterized by a complex terrain (Fig. 1a). Main features of the area under study include: (1) the coastal depression which contains most of the cities in the Barcelona metropolitan area in the 8-km strip of land between the sea and the first mountain range; (2) the coastal mountain range with main peaks around 500–650 m (Collserola Hills, Fig. 1); (3) the pre-coastal depression between the mountain coastal ranges and (4) the pre-coastal mountain range where the regional background (RB) station is located (Fig. 1).

M. Dall'Osto et al.

Title Page

Abstract	Introduction
Conclusions	References
Tables	Figures

◄◄   ►►

◄   ►

Back   Close

Full Screen / Esc

Printer-friendly Version

Interactive Discussion

With a population of about 1.7 million inhabitants in the city and around 4 millions in the metropolitan area, Barcelona is the fifth most populated metropolitan area in Europe. The urban architecture and dynamism around Barcelona city account for the highest population density in Europe (about 16 000 inhabitants km^{-2}); reflected also in the highest road traffic density (6100 cars km^{-2}, much more than in most European cities with about 1000–1500 cars km^{-2}) (Amato et al., 2009; Reche et al., 2011). Additionally, Barcelona has one of the main harbors in the Mediterranean Basin, with the highest number of cruise ships for tourists in Spain, being a potential focus of emissions of atmospheric pollutants. Furthermore, several industrial zones, power plants, and important highways cross the area in all directions. In this situation, anthropogenic emissions are of a high importance and make this region one of the most polluted in the WMB.

A key feature of the SAPUSS study was the number of monitoring sites used, six in total: supersite Road Site (RS), supersite Urban Background (UB), site Tower Mapfre (TM), site Tower Collserola (tower and ground urban background TC and TCg, respectively), and site Regional Background (RB) (Fig. 1). RS and UB were named "supersites" as a large variety of instruments were deployed relative to the remaining sites. Table 2 shows the list of the instruments deployed during the SAPUSS field study.

2.1 Supersite road site (RS)

The RS site (41° 23′ 18″ N; 02° 09′ 0″ E, Fig. 1) was situated in the car park of the Escuela de Ingeniería Técnica Industria (St. Urgell, 187 – elevation 40 m a.s.l.). Most instruments were located inside three vans parked about 4 m from the curb. Air was drawn from outside to the instruments throughout a number of home designed inlets, situated on the van's roofs at a height of about 4 m above ground with 1/4 inch stainless steel tube led inside each trailer (length about 2 m) to a manifold. Other off-line instruments were directly measuring aerosol properties without deploying any inlets.

Some light trees, a fence and a 2 m wide pedestrian path separated the road from the monitoring instruments. The road, which cuts the city from south east to north west,

is a street canyon composed by a two-way cycling path and a one-way four lane vehicle road. Fig. 2a shows the vehicle intensity during the month of measurements, with an hourly average intensity of 690 ± 370 vehicles (about 17 000 vehicles day^{-1}), reaching up to 1050 ± 420 vehicles per hour during traffic rush hours (Fig. 2b). A subway entrance is located on the right side of the RS, whereas shops and restaurants can be found opposite the RS. Two traffic lights are located about 50 and 150 m away from the RS, on the right and left side, respectively.

2.2 Supersite urban background site (UB)

The UB measurement site ($41° 23′ 15″$ N, $02° 07′ 05″$ E, Fig. 1) was situated at the north western periphery of the city centre in a small park (elevation 80 m a.s.l.). It is mainly surrounded by residential areas and it is situated about six km from the sea (Fig. 1). Two trailers were deployed for housing the instruments at the UB, and the inlets (like the ones described for the RS site) were also situated on the roof of the two trailers at about 4 m above ground. It is important to remember that at a distance of about 300 m from the UB is Diagonal Avenue, one of Barcelona's broadest and most important avenues (nine vehicle lanes in total). During the SAPUSS field study, the hourly average vehicle intensity was 2560 ± 1300 (62 000 vehicles day^{-1}), going up to 5100 ± 1700 during the 8 a.m. traffic rush hour peak. Note that the vehicle intensity (Fig. 2a) and the occupancy (Fig. 2b) of this main road present strong peaks at 8 a.m. (7–9 a.m.) and 6 p.m. (5–8 p.m.). This diurnal variation is different from the one of the road next to the RS site and the reason is due to the fact that whilst the Diagonal Av. is mainly used for commuting in and out the city during the day, the road next to the RS (St. Urgell) reflects more the commercial traffic activity of the urban city centre.

2.3 Tower Mapfre site (TM)

Name after its owner, Torre Mapfre ($41° 23′ 16″$ N, $2° 11′ 51″$ E, Fig. 1) is a skyscraper in the Olympic Port, the maritime neighbourhood of the Old City of Barcelona. This

tower holds the title for highest helipad in Spain at 154 m above ground (154 m a.s.l.). It is located about 200 m from the sea, with a small marina, a dock or basin with moorings and supplies for yachts and small boats in the south east corner. The south west corner instead is characterized by a well known Barcelona recreational area. By contrast, in the North side of the tower the ring road motorway B-10 (Ronda del Litoral) can be found, a two-lane both ways road (four lanes in total). The B-10 is tunneled about 250 m before and after the tower (0.5 km in total). Powerful air ventilators constantly renew the air and maintain the air quality within the tunnel motorway and the extraction of the exhaust fumes is located next to the TM. Adjacent to the B-10, two additional three-lane roads can be found at ground level (above the tunnelled B-10). Aerosol measurements were taken at the top floor of the tower (150 m a.s.l.). Instruments were deployed on the terrace of the tower, whereas some of the instruments were stored inside a room at the top floor (with 0.5 m 1/4 inch copper pipe linked to the outside).

2.4 Tower Collserola sites (TC and TCg)

Collserola is a mountain range (Tibidabo being the tallest peak, at 512 m) between the Besòs and Llobregat rivers (Fig. 1). It is part of the Catalan Coastal Range, and such mountains separate Barcelona from the Vallès plain (pre-coastal depression). The area is preserved as Park (Collserola Park, 84.65 km^2) and is the largest metropolitan park in the world. On the Vilana hill stands the Torre de Collserola (Collserola Tower, 41° 25′ 02″ N, 02° 06′ 51″ E, Fig. 1), a telecommunications tower built in 1992 for the Olympic Games. The tower is located at 445 m a.s.l., and measurements were taken on the fourth floor of this tower, at 80 m above ground level (525 m a.s.l.). Instruments were kept inside a room, and short inlets (< 1 m 1/4 inc copper pipe) were used to sample ambient air. Due to logistical reasons at the TC site (limited access and storage space), the Fabra Observatory (41° 25′ 56″ N, 2° 07′ 27″ E) was also used as a monitoring site during the SAPUSS project. The Fabra Observatory is an astronomical observatory at 415 m altitude above sea-level of the sea, and located about 450 m (900 m road distance) from the TC site. In summary, measurements were taken at ground level

(TCg, 10 m above ground, 425 m a.s.l.) and at tower level (TC, 80 m above ground, 525 m a.s.l.). Is is important to note that whilst TM is well within the Barcelona urban city centre, TC is located in the hills of the urban background of Barcelona.

2.5 Montseny regional background site (RB)

The Montseny site (41° 46′ 45″ N 02° 21′ 29″ E, Fig. 1) is part of the EUSAAR network (European Supersites for Atmospheric Aerosol Research, abbreviation "MSY"). The RB monitoring site is located within a regional natural park at about 50 km to the North-North East side of the city of Barcelona and about 30 km from the Mediterranean coast. The Montseny natural park has the highest mountains in the area south of the Pyrenees and dominates the plains south of Girona. A detailed description of the measurement sites and previous measurement of aerosol concentration and composition can be found in the literature for the MSY station (Pey et al., 2010).

3 Description of measurements

3.1 Physical properties

3.1.1 Meteorological parameters

Meteorological variables (atmospheric pressure, wind speed WS, wind direction WD, solar radiation, temperature and relative humidity) were recorded at five SAPUSS monitoring sites (all excluding TC) during the whole field study. Data for RS, TM, TCg and RB were obtained from instruments located within the monitoring sites, whereas data for UB were obtained from a close meteorological station (100 m distant from our UB measurement site) located on the roof terrace of the Chemical and Physical Sciences Faculty of the Barcelona University.

Some meteorological data were compromised, including: data from the TM site, which was under the shadow of the top part of the tower in the afternoon (affecting the

solar radiation, the RH and the temperature values); and wind data from the RS site, which were affected by the street canyon conditions found in the road site (although representative of a typical road in Barcelona).

3.1.2 Remote sensing measurements

The planetary boundary layer (PBL) above Barcelona was monitored by simultaneous measurements of two Jenoptik CHM15K LIDAR ceilometers (Heese et al., 2010; Martucci et al., 2010) with 1064-nm wavelength and 15-km vertical range. The first ceilometer was deployed vertically and it was located in the South West part of Barcelona, on the roof terrace (8 m above ground) of the Institute of Earth Sciences "Jaume Almera" (Consejo Superior de Investigaciones Cientificas: CSIC), about 300 m south from the UB site. The second ceilometer was deployed horizontally on the terrace of the Fabra observatory, looking at the Torre Mapfre (TCg, TM, Fig. 1).

The PBL height and vertical structure was retrieved with standard 30 s and 15 min temporal and vertical resolution, respectively, by applying the Temporal-Height-Tracking (THT, Martucci et al., 2010; Haeffelin et al., 2011) algorithm to the LIDAR returns from the CHM15K. The THT is 1-D (spatial) gradient and time-constrained technique to retrieve the PBL structure. It is important to remember that the vertical profiles of atmospheric temperature, pressure and relative humidity as well as wind components were also obtained by radiosoundings performed twice per day (at 12:00 UTC and 00:00 UTC) at the UB site.

3.1.3 Total and size-resolved particle number concentrations

Total particle number concentrations were measured at 5 SAPUSS monitoring sites (RS, TM, TC, RS, UB). The same type of CPC particle counter (TSI CPC Model 3022A; lower 50 % cut-point 7 nm) was simultaneously deployed at the RS, TM, TC sites, whilst the instruments at the RB and UB sites were a TSI water based (WB) CPCs 3785 (with a lower 50 % cut-point at 5 nm) which would lead to slightly higher readings relative

to the Model 3022A instrument (Table 2). Instruments were intercompared before and after the campaign, giving excellent overlaps, with uncertainty of about 5 % both before and after the campaign. Nano CPCs (TSI 3025 and TSI WB 3786, 50 % cut-point at 3 nm) were also partially available during the SAPUSS project (Table 2). A number of different SMPS systems were deployed simultaneously at 4 different sites (RS, UB, TCg, RB, Table 2), providing size resolved aerosol particle number concentrations.

3.1.4 Aerosol mass loadings

Aerosol mass loadings were determined both gravimetrically and by using real time optical counters. As regard for gravimetric measurements, high volume samplers DIG-ITEL DHA-80 and MCV CAV-A/Mmb ($30 \, \mathrm{m^3 \, h^{-1}}$) equipped with PM_1 or PM_{10} heads collected 12 h samples (from 11 a.m. to 11 p.m. and from 11 p.m. to 11 a.m., LT) on quartz fiber filters (Pallflex 2500QAT-UP). PM_{10} samples were collected at five SA-PUSS sites (RS, UB, TCg, TM, RB), whereas PM_1 samples were collected only at RS, UB and RB sites. 24 h $PM_{2.5}$ samplers were collected at the UB and RS site. The total number of high volume samplers collecting PM during the SAPUSS was 10 (Table 2). The gravimetric mass concentrations were corrected to account for humidity saturation on the filter. PM_{10}, $PM_{2.5}$ and PM_1 concentrations were also continuously measured by means of optical counters dust monitors (Grimm Labortechnik GmbH & Co. KG; model 1107). The different instruments were intercompared before the campaign, and the one from TCg was corrected according to the concentrations registered by the instruments deployed at TM and TC. The Grimm PM concentrations were also corrected with the corrected gravimetric PM concentrations.

Presenting SAPUSS

M. Dall'Osto et al.

Title Page

Abstract | Introduction

Conclusions | References

Tables | Figures

|◄ | ►|

◄ | ►

Back | Close

Full Screen / Esc

Printer-friendly Version

Interactive Discussion

3.2 Chemical properties

3.2.1 Real time (on-line) techniques

Black Carbon mass derived by aerosol absorption

Black Carbon mass was derived by Aerosol absorption using both a McGee Scientific Aethalometer AE-16 (Aet.) and a Multi-Angle Absorption Photometer (MAAP). A total of 4 MAAP instruments were deployed during the SAPUSS (RS, UB, TC, RB, Table 2) whereas an Aethalometer was deployed at the TM site. MAAP instruments gave excellent agreement between them (±5 %). The MAAPs and the Aethalometer were inter compared before and after the field study, also giving excellent agreement (fitting: Aet = 0.85 × MAAP, 505 points, R^2 = 0.98).

ATOFMS

The TSI ATOFMS collects bipolar mass spectra of individual aerosol particles. Two types of instruments are currently available, depending on the inlets used for bringing particles into the ATOFMS vacuum system: a nozzle/skimmers combination (older TSI Model 3800) and a set of aerodynamic lenses (newer TSI Model 3800-100). Whilst the efficiency of the former is heavily biased towards the super micron aerosol (Gard et al., 1997), the latter focuses a narrow particle beam for sizes between 100 nm and 3 µm (Su et al., 2004). The ATOFMS provides information on the abundance of different types of aerosol particles as a function of particle size with high time resolution (Suess and Prather, 1999; Su et al., 2004). ATOFMS can also provide quantitative chemical information if a relative sensitivity factor is applied (Gross et al., 2000; Dall'Osto et al., 2006; Qin et al., 2006). Two ATOFMS were deployed simultaneously during the SAPUSS field study at the RS (TSI 3800-100, aerodynamic lens) and at the UB (TSI 3800, nozzle/skimmer), respectively.

Presenting SAPUSS

M. Dall'Osto et al.

HR-Tof-AMS

The HR-ToF-AMS (De Carlo et al., 2006) focuses aerosol particles in the size range 50–600 nm quantitatively onto a hot surface (600 °C) using an aerodynamic lens assembly (Jayne et al., 2000). Smaller and larger particles are also collected with lower efficiency. Non-refractory particle components flash-evaporate on the hot surface; the evolving vapour is electron impact (70 eV) ionized and the ions are transported into an orthogonal extraction ToF-MS for high-resolution mass analysis. Particle size information is obtained by chopping the particle beam and collecting mass spectra as a function of particle flight time. Two HR-ToF-AMS were deployed during the SAPUSS, co-located next to the two ATOFMS at the supersites RS and UB.

3.2.2 Off-line chemical analysis techniques

Standard IDAEA-CSIC filter analysis

PM mass concentrations were determined by standard gravimetric procedures as described in Sect. 3.1.4. Filter samples were collected and analyzed following the procedures described by Querol et al. (2001b): Al, Ca, K, Mg, Fe, Ti, Mn, P, S, Na and 25 trace elements by conventional methods including inductively coupled plasma atomic emission spectrometry and mass spectrometry (ICP-AES and ICP-MS, respectively), SO_4^{2-}, NO_3^- and Cl^- by ion chromatography (IC), and NH_4^+ by selective electrode. A section of 1.5 cm^2 of the filter was used for the determination of organic carbon (OC) and elemental carbon (EC) by a thermaloptical transmission technique (Birch and Cary, 1996) using a Sunset Laboratory OCEC Analyzer with the EUSAAR2 temperature program (Cavalli et al., 2010). Additionally, 1/8 part of the filter was ultrasonically extracted in a mixture of dichloromethane and methanol (2 : 1, v/v). Surrogate standards were added to samples for analysis of anhydrosugars, dicarboxylic acids, polycyclic aromatic hydrocarbons and hopanes. Extracts were filtered concentrated to 1 ml. Aliquots of 25 µl of the extract were derivated with bis(trimethylsilyl)trifluoroacetamide

(BSFTA)+trimethylchlorosilane (99:1) (Supelco, USA) and 10 μl of pyridine (Merck, Germany) for analysis of the methylsilylate esters of levoglucosan and dicarboxylic acids together with nicotine. All sample extacts were analyzed by gas chromatography coupled to a mass-spectrometer (GC-MS).

Streaker particle induced X-ray emission (Streaker-PIXE)

Hourly elemental concentrations were obtained at the RS and UB by a two stages (0.1–2.5 μm and 2.5–10 μm, fine and coarse, respectively) streaker sampler. Full details of the sampler, its cut-off diameters, control unit, etc. can be found elsewhere (Formenti et al., 1996). 640 hourly samples were collected and analyzed by PIXE at the LABEC-INFN facility in Florence (based on a 3 MV Tandetron accelerator, where an external beam set-up is fully dedicated to atmospheric aerosol studies; Chiari et al., 2005). X-ray spectra were analysed for 25 elements (Na, Mg, Al, Si, P, S, Cl, K, Ca, Ti, V, Cr, Mn, Fe, Ni, Cu, Zn, As, Se, Br, Rb, Sr, Zr, Mo and Pb) using the GUPIX software package (Maxwell et al., 1995) and the elemental concentrations were obtained via a calibration standards certified within 5 % (Micromatter Inc.).

3.2.3   Gaseous pollutants: O_3, NO, NO_2, CO, SO_2, NH_3

Standard continuous gas measurements were taken for SO_2 (UV fluorescence), NO-NO_2-NO_x (chemiluminescence), CO (IR absorption) and O_3 (UV absorption) at four sites (RS, UB, TCg, RB). Atmospheric NH_3 levels were determined by means of AL-PHA passive dosimeters (Adapted Low-cost Passive High Absorption sampler; Tang et al., 2001) at all six monitoring sites. The ALPHA samplers are made up of a circular polyethylene vial with one open end, which contains a phosphoric acid coated filter to capture ambient ammonia. A PTFE membrane is placed before the filter, allowing gaseous NH_3 to diffuse through. The samplers were deployed at each of the monitoring sites, with an exposure time of seven days. After exposure, samples were analysed in-house by means of a NH_4^+ selective ion electrode after filter extraction in 3 ml of

Presenting SAPUSS

M. Dall'Osto et al.

deionised water. Laboratory blanks were analysed following the same procedure as ambient samples. The total number of samples collected was 4 samples site^{-1} at TM, UB, RS and TCg, and 2 samples site^{-1} at RB and TC.

3.3 Modelling activities

3.3.1 Air mass back trajectories analysis

The study area is affected by convergence of air masses with different characteristics: the cold air coming down from medium and high latitudes, and the warm air coming up from tropical and subtropical latitudes. Back trajectories of the air masses arriving at Barcelona were calculated four times for each day of the campaign (00:00, 06:00, 12:00 and 18:00 UTC), depicting the path taken by the air mass reaching the sampling site over the previous five days. The back trajectories were run using the on-line HYSPLIT model developed by the National Oceanic and Atmospheric Administration (NOAA) (Draxler, 2003). Air mass "types" are usually classified according to latitude and their continental or maritime source regions (Bergeron classification). However, during SAPUSS air mass back trajectories "scenarios" names given will also be used, including: Atlantic (ATL), European-Mediterranean (EUR), North African (NAF) and Regional (REG) scenarios (Rogriguez et al., 2002; Pey et al., 2010).

3.3.2 Chemical transport models

The modeling system consists of the Fifth-Generation Pennsylvania State University – National Center for Atmospheric Research Mesoscale Model (MM5) (Dudhia, 1993; Grell et al., 1994) coupled to EMEP emissions (Vestreng et al., 2007) (disaggregated to the working resolution following a methodology analogous to Pay et al., 2010) and to CHIMERE chemistry transport model (Schmidt et al., 2001; Bessagnet et al., 2004; Rouil et al., 2009). MELCHIOR2 gas-phase mechanism is implemented within CHIMERE (Derognat et al., 2003). The chemistry transport model (CTM) includes

Full Screen / Esc

aerosol and heterogeneous chemistry; distinguishes among different chemical aerosol components, namely nitrate, sulfate, ammonium, elemental and organic carbon with three subcomponents (primary, secondary anthropogenic and secondary biogenic) and marine aerosols. Unspecified primary anthropogenic aerosols and aerosol water are additionally kept as separate components. The model considers the thermodynamic equilibrium using the ISORROPIA model (Nenes et al., 1998). Last, the aerosol microphysical description for CHIMERE is based on a sectional aerosol module including 6 bins from 10 nm to 40 µm using a geometrical progression. Further description of the modeling system can be found in Jiménez-Guerrero et al. (2011a, b).

4   Results

4.1   Air mass back trajectories analysis

Five air masses scenarios were classified during the SAPUSS field study (Fig. 3). Table 3 shows that 23 days during SAPUSS presented the same air mass type within the 24 h of each day, whereas days with multiple air mass types within the same day were classified as "transition" (Table 3, Fig. 3). It is important to clarify that the classification was made not only accordingly to air mass back trajectories, but also by looking at the local meteorological data available at the five sampling sites.

4.1.1   Regional air mass (REG)

A typical REG air mass scenario is shown in Fig. 3. This air mass type (Continental Polar) was found the one occurring most frequently during the SAPUSS field study, occurring for a total of 9 days. Three distinct episodes were found: 20–21 September, 29 September–1 October and 14–17 October. Regional air masses are typical during the summer months in the Western Mediterranean, with higher temperatures and greater insolation (Millan et al., 1997). The Azores anticyclones dominate the pressure system and, at the same time, large thermal low systems develop over the Iberian

Title Page

Abstract | Introduction

Conclusions | References

Tables | Figures

◄ | ►|

◄ | ►

Back | Close

Full Screen / Esc

Printer-friendly Version

Interactive Discussion

Peninsula with land-sea breezes being very active over the coasts (Millan et al., 2000). These regional episodes are developed under meteorological scenarios characterized by a lack of a significant synoptic air mass advection. Whilst the schematic of the complex development of mesoscale atmospheric recirculation has already been presented in great detail (Millan et al., 2000), a conceptual figure with the SAPUSS monitoring sites is presented in Fig. 1c. Finally, Fig. 4 shows average temperature and RH and lower WS for this air mass type (relative to the others).

4.1.2 Atlantic air mass (ATL)

ATL air mass scenario (Marine Polar air type) occurred second most frequently during the SAPUSS project, characterizing a total of 7 sampling days. ATL scenarios possess intensive advections from the Atlantic Ocean, associated with cold fronts crossing the IP. Meteorological values for this air mass type showed the driest conditions recorded during the study (Fig. 4a) associated with the coldest temperatures (Fig. 4b), sunny days (Fig. 4c) and strong northerly winds (Figs. 4d, 5).

4.1.3 European air mass (EUR)

This air mass scenario originated in the East side of the European continent (Continental Polar air mass type) and crossed all Europe before arriving in Spain. Such conditions began at 8 a.m. on the 11 October lasting continuously for more than two days till 3 p.m. on the 13 October (Fig. 3). The transport of particulate pollutants from mainland Europe has already been reported as potential scenario for high PM episodes, although wet/rainy weather situations and strong winds favoring pollutant dilution and scavenging may also show an opposite trend (Rogriguez et al., 2002). Figure 4a shows that the EUR air mass scenario is characterized by the wettest conditions of the entire SAPUSS field study, lowest solar radiations (Fig. 4c) and strongest wind (Fig. 4d) from Easterly directions (Fig. 5).

4.1.4 East and West North African air mass (NAF_E and NAF_W)

Three events (six days in total) were found for this Continental/Marine Tropical air mass type (Fig. 3). Those air masses were found to be the warmest ones encountered during the SAPUSS campaign (Fig. 4b), about 4 °C warmer than any other air mass type. According to Escudero et al. (2005), four meteorological scenarios originate the transport of African dusty air masses towards the WMB: (1) a North African high located at surface levels (NAH-S), (2) an Atlantic depression (AD) situated in front of Portugal, (3) a North African depression (NAD), and (4) a North African high located at upper levels (NAH-A). During the SAPUSS, two different NAF air mass scenarios were classified and named as NAF_E and NAF_W, respectively. Figure 3 shows an air mass trajectory originated in the Tropical Atlantic Ocean and arriving from the South West direction to Barcelona (NAF_W) (Figs. 3, 5). By contrast, the NAF_E air mass type originated in the Saharan region and arrived at Barcelona from the Easterly wind sector, as clearly seen in the associated wind roses (Fig. 5).

4.2 Local meteorology

Meteorological conditions during SAPUSS appear in Fig. 4. Average temperatures at the urban ground sites (RS 20.6 °C and UB 18.7 °C) were found higher than the other sites, due to the urban heat of the city, whereas colder temperatures were found both at higher altitudes and remote regional sites (TCg 16.5 °C and RB 14.1 °C). Figure 6 shows the diurnal profiles of T (Fig. 6a), RH (Fig. 6b), solar radiation (Fig. 6c) and WS (Fig. 6d) for all SAPUSS sampling period. Typical diurnal profile can be seen for RH and T at all sites, with the ground urban ones (RS and UB) presenting the strongest day/night variation. For all the monitoring sites, the warmest part of the day was found at 3 p.m. in the afternoon. The solar radiation cycle started at about 7 a.m. and terminated at about 8 p.m. (Fig. 6). During the SAPUSS, the sun rose at 07:36–08:08 a.m. and the sun set at 07:06–07:54 p.m. (local time, UTC + 2). Figure 6 shows that not only TM but also the RS site is affected by the shadows of nearby buildings.

As regard of WS, Fig. 6d showed the strongest wind speed at TCg (4.2 m s^{-1}), followed by the UB site (2.4 m s^{-1}). Whilst the RS site presented generally low WS (lacking of a clear diurnal trend due to its street canyon characteristic), the UB and RB shows typical diurnal variations associated with the sea breeze patterns. However, opposite trends are seen for the TCg. The sea breezes (usually originating from about 60° and moving towards a dominant the 120° −180° sector) are at their strongest around midday, when the boundary layer height maximizes (Perez et al., 2004).

As regard of wind roses, different wind pattern scenarios were found under different air masses scenarios (Fig. 5). Northerly winds are seen for the UB and TC sites. By contrast, giving the fact that the WS at the RB and RS were often below 2 m s^{-1}, WD data for these sites are indeed more variable and do not really allow any firm conclusion to be drawn. Finally, Fig. 7 summarizes the WS and the WD diurnal patterns for representative days of the five air mass scenarios described in Sect. 4.1:

– ATL (25 September 2010, Fig. 7a): Atlantic air masses are characterized by strong winds from the north east–north west sector for the RS and UB urban sites. Whilst uncommon during winter times, during summer times the sea breeze scenario can occur, as seen in the RB site.

– EUR (12 October 2010, Fig. 7b): This is a very peculiar air mass type, with strong wind coming mainly from the east sector. The absence of sea breeze circulation is also a key feature of this air mass type.

– REG (30 September 2010, Fig. 7c): A typical sea breeze pattern is seen at all sites, although not at the TCg site.

– NAF_W (3 October 2010, Fig. 7d): Strong South west direction remarkably constant during all day for all sites. The sea breeze blowing from the same Westerly direction enhances the WS during the warmest part of the day.

– NAF_E (9 Otober 2010, Fig. 7e): A remarkable Easterly WD is observed during all day at both TC and UB sites. The RB site also shows an Easterly WD during the

Presenting SAPUSS

M. Dall'Osto et al.

Title Page

Abstract	Introduction
Conclusions	References
Tables	Figures

|◄ | ►|

◄ | ►

Back | Close

Full Screen / Esc

Printer-friendly Version

Interactive Discussion

warmest part of the day when the see breeze blows wind into the Besos Valley (see map in Fig. 1a).

4.3 Planetary boundary layer characterization

The PBL is the atmospheric region with the highest concentration of aerosols between the ground level and the free troposphere, and where aerosols experience turbulent mixing and are homogeneously distributed. Terminology is often a problem so here we define the layer nearest the surface, which is typically well mixed, as the surface mixed layer (SML), noting that this layer can deviate from being well mixed (i.e. neutral stability), and the layer occupying the region below the Free Troposphere inversion as the decoupled residual or convective (DRC) layer. The PBL heights obtained from the ceilometer (ciel.) positioned vertically the ground were compared with those obtained from radio sounding balloons data (Rad.S) at noon and a good correlation was found (Rad.S = 0.8 · ciel. + 100; R^2 = 0.74). A total of 730 h (30 days) of PBL heights (SML and DRCL), backscatter coefficients and meteorological data were collected during the SAPUSS campaign. The values of the SML and DRCL during the SAPUSS study ranged between 430 and 1916 m a.g.l. and between 829 and 2543 m a.g.l. (respectively), in agreement with previous measurements (Sicard et al., 2011; Perez et al., 2004). Mean values during SAPUSS, once excluded data with rain and/or low clouds, were 879 ± 264 m for the SML and 1747 ± 355 m for the DRCL, respectively. Backscatter coefficients at 400 m and 800 m a.s.l. within the ranges $4.1 \times 10^{-8} \div 8.2 \times 10^{-6}\,\mathrm{m}^{-1}\,\mathrm{sr}^{-1}$ and $1.3 \times 10^{-8} \div 1.1 \times 10^{-4}\,\mathrm{m}^{-1}\,\mathrm{sr}^{-1}$, respectively were measured. Mean values were $5.0 \pm 6.1 \times 10^{-7}$ at 400 m a.g.l. and $3.2 \pm 8.8 \times 10^{-6}\,\mathrm{m}^{-1}\,\mathrm{sr}^{-1}$ at 800 m a.g.l. Figure 8 shows the first continuous measurements of SML and DRCL taken in Barcelona, where a clear diurnal cycles is seen peaking during the warmest hours of the day.

4.4   Level of gaseous pollutants

Table 4 reports the average concentrations for all gases at five different monitoring sites. Please note that the only gaseous measurement taken at the TM site was for NH_3, whereas the other four sites present a wider data coverage.

4.4.1 NH_3

Table 4 shows remarkably higher mean NH_3 levels at the urban sites (RS, UB and TM), ranging between 2.0 and 3.1 $\mu g\,m^{-3}$, when compared to the levels detected at the background sites TC and TCg. (1.0–1.1 $\mu g\,m^{-3}$) and in the regional background (RB, 0.5 $\mu g\,m^{-3}$). A certain gradient is even evident among the urban sites, increasing from 2.0 to 3.1 $\mu g\,m^{-3}$ from the urban background (UB) to the traffic environment (RS), pointing to a vehicular traffic as a main source influencing the spatial variability of atmospheric ammonia among the study sites. It is interesting to note that the NH_3 levels registered at the TC and TCg sites are within one standard deviation of each other, as it would be expected given that these sites are located in close proximity to each other. Mean NH_3 levels at TM and UB sites are also similar, despite the markedly different environments. The TM site is located above the ground but in proximity of a busy motorway whereas the UB site is located at ground level but in the background urban area. Overall, ammonia concentrations detected in Barcelona were of the same order of magnitude as those detected in Houston, USA (2.1 $\mu g\,m^{-3}$, Gong et al., 2011) but much lower than the ones detected in Beijing, China (14 $\mu g\,m^{-3}$, Meng et al., 2011). Finally, it is important to note that urban NH_3 average concentrations in Barcelona (summer 9.5 $mg\,m^{-3}$, winter 4.4 $mg\,m^{-3}$) are higher than those reported in other urban background sites in Europe (Reche et al., 2012).

4.4.2 Other gaseous pollutants

Traffic markers such as NO and CO showed as expected highest values at the RS site ($8.8 \pm 12\,\mu g\,m^{-3}$ and $0.4 \pm 0.3\,\mu g\,m^{-3}$, respectively, Table 4) and lowest values towards the RB site following the order RS, UB, TCg and RB, respectively and representative of the higher distance from hot spot traffic sources.

Although low in absolute value, SO_2 levels were also found to be the highest at the RS traffic site ($2.1\,\mu g\,m^{-3}$), as a direct effect of exhaust emissions. Lower SO_2 were generally found in Barcelona when compared to other European cities (Reche et al., 2011) as power plants around the city combust with natural gas. Interestingly, higher concentrations of SO_2 are seen at the tower site TCg relative to the UB and RB ground sites. This is likely to be due to regional range transport of SO_2 from industrial areas situated in the north part of the Barcelona metropolitan area, although the port of Barcelona is also a main source (Pey et al., 2010). During some stagnant air masses conditions (29 September–1 October) higher levels of SO_2 were found at the TCg site above the city of Barcelona relative to ground site (RS and UB), pointing towards a stratification of SO_2 over the Barcelona urban areas.

Ozone presented also as expected the lowest values at the RS ($43 \pm 21\,\mu g\,m^{-3}$) and the UB ($58 \pm 22\,\mu g\,m^{-3}$) as a consequence of a major consumption of O_3 by NO. However, higher values of ozone were found at the TCg relative to the RB despite the higher levels of NO_x at the former site (Table 4). More considerations on ozone concentrations during the SAPUSS are given in the next section (Sect. 4.4.3).

Figure 9 shows the hourly diurnal temporal trends calculated for the five gas pollutants monitored simultaneously at the four different sites:

– NO at the city ground sites of UB and RS shows a trend linked with the traffic activity. At the UB, a strong maximum is seen at 8 a.m. partly due to the strong influence of busy Diagonal Av. By contrast, the RS shows a spike at 9 a.m. which decreases only moderately at about 1 p.m., until it increases again during the evening traffic rush hours at around 5–10 p.m. NO diurnal temporal trends for

the TCg site are shifted (relative to the UB and RS sites) as the maximum concentrations are detected only when the boundary layer is fully developed between 10 a.m. and 2 p.m. allowing the city pollutants to be transported to the background TCg site. For the same reasons, the regional site (RB) shows a peak at about 1 p.m., lasting for about four hours till about 5 p.m.

– CO shows a similar trend of NO at all sites, confirming its main traffic source. However, a spike at about 1 p.m. is seen at the RS and it is associated to unknown non traffic combustion sources. At the RB site, CO presented a similar trend like the one seen for NO, whereas a second spike was seen for the more urban background TCg site at about 18–20.

– NO_2 presented a different daily pattern relative to NO, with a second spike during 7 p.m.–9 p.m. for both the RS and the UB. At TCg, the morning spike is shifted towards the 11 a.m.–1 p.m. window, when the boundary layer is fully developed. By contrast, the evening spike at 5 p.m.–8 p.m. is decreased in intensity due to lower boundary layer conditions.

– SO_2 diurnal trends were not well defined during the SAPUSS project, with noisy diurnal trends. Whilst the RS seem to reflect the traffic conditions, at the UB site the SO_2 concentration peaks in the afternoon, reflecting previous studies (Reche et al., 2011). At the TCg site the highest SO_2 concentrations were found during night time.

– Ozone values were found to be linked with NO_x levels at UB and RS. Higher values of O_3 were found at the TCg for most of the night time periods (see Sect. 4.4.3).

When levels of gaseous pollutants from different air mass scenarios are compared, the sea breeze was found a key parameter governing their concentrations levels. A sea breeze in the topographic and regional context of the WMB may exacerbate air pollution levels by constricting local ventilation and instead recirculating air around multilayered

Presenting SAPUSS

M. Dall'Osto et al.

Title Page

Abstract | Introduction

Conclusions | References

Tables | Figures

|◄ | ►|

◄ | ►

Back | Close

Full Screen / Esc

Printer-friendly Version

Interactive Discussion

pollution closed cells. On the other had, a sea breeze may move relatively clean air onshore that will rapidly lower gas concentrations. Figure 10 shows the diurnal temporal trends for selected gas phase pollutants at the four different monitoring sites according to different air mass scenarios. During morning hours, when the air is still, pollutants can accumulate over their sources or downwind of them. Later in the day, when a local sea breeze develops, a fresh breeze blows in the direction from the sea (120–180°) toward land. In addition to this effect, which generally occurs close to land, the sea breeze itself can penetrate as far inland throughout the two valleys (Llobregat and Besos, Fig. 1), reaching the RB site.

REG and NAF_W air masses were found to present the highest levels of NO and NO_2 at the UB and RS sites. During NAF_W air masses pollutants are transported at high concentrations from the city towards the TC and RB sites due to the favorable wind patterns: strong Westerly wind blowing parallel to the Besos valley (Fig. 1). By contrast, ozone presented a similar trend at the RS and UB for mostly air masses, mainly spiking in the afternoon. However, unusual conditions were found for European air masses, with less diurnal variation due to the contribution of regional transport and reduced local traffic sources during raining conditions. After sunrise, the height of the unstable boundary layer begins to increase as the surface is heated and the nocturnal inversion is destroyed, resulting in downward mixing O_3 from above. This may be the reason why there is an increase of ozone in the morning at some of the sampling sites under this EUR air mass scenario (Fig. 10, De Foy et al., 2006).

4.4.3 O_3/NO_x chemistry and oxidant plot

The classic concept of upwind (background concentrations) and downwind of conurbations (polluted) is inappropriate in regions of complex coastal terrain like the WMB, where recirculation processes are important. Indeed, a number of studies have shown that mainly during summer the layering and accumulation of pollutants such as tropospheric ozone (Seinfeld and Pandis 1998; Tong et al., 2011) and aerosols take place along the WMB coast (Millán et al., 1997, 2000; Jorba et al., 2004), as result

of the complex interaction between breeze circulation and topographic heights. Díaz-de-Quijano et al. (2009) also suggested that the ozone in the Catalan Pyrenees mainly originated from urban areas, which is then transported to high-mountain sites, remaining aloft in absence of NO. Furthermore, a number of multiscale modelling simulation results over Barcelona additionally show that the strength of the land-sea breeze circulation and thermally or mechanically driven convection over the complex orography of the Eastern Iberian coast can induce vertical transport and the layering of air pollution (Millan et al., 1997; Toll and Baldassano, 2001; Jimenez et al., 2006).

During the SAPUSS field study, the average ozone concentration for the Gencat "regional" air pollution monitoring stations from Catalunya (7 stations: Bellver de Cerdanya, Berga, Ponts, Sant Celoni, Santa Maria de Palautordera, Santa Pau, Sort) was found to be $55 \pm 10\,\mu g\,m^{-3}$ (max. value $114\,\mu g\,m^{-3}$); and its average diurnal profile is presented in Fig. 11a. The ozone diurnal variation at the urban ground level for the RS and UB sites show a typical urban pattern: minimum levels during morning traffic rush hours and maximum in the afternoon (Fig. 11a). The level of ozone at the regional RB site shows overall higher average concentrations during night time, indicating a residual layer of ozone maintaining at higher altitude in the Besos valley. Higher values relative to other regional sites were also found at Pardines ($69 \pm 15\,\mu g\,m^{-3}$, max $118\,\mu g\,m^{-3}$), a station further away from Barcelona at the very top north west end of the Besos valley (Fig. 1). During the afternoon, when the boundary layer is fully developed, the levels of ozone at UB, RB and TC are similar at about $80\,\mu g\,m^{-3}$.

By contrast, under stable nocturnal boundary layer conditions higher level of ozone were found at the TCg site above the urban area of Barcelona. The reason is likely due to the fact that turbulence and vertical mixing are strongly suppressed in the nocturnal boundary layer, therefore emissions at the ground are only slowly transported vertically resulting in vertical concentration gradients for many trace gases, making nocturnal chemistry dependent on altitude and vertical stability (Wong and Stutz, 2010).

Figure 11b shows an "oxidant plot", where the level of total oxidant ($OX = O_3 + NO_2$) is plotted as a function of NO_x ($NO + NO_2$). Oxidant plots such as these have been

interpreted as showing both the regional background oxidant (ozone) level, indicated by the y-axis intercept, and the local primary contribution to oxidant (potentially primary NO_2 emissions), indicated by the gradient (Clapp and Jenkin, 2001).

It is important to remember that ozone values in Table 4, Figs. 10 and 11 a are in $\mu g\,m^{-3}$, whereas Fig. 11 b shows data in ppb (1 ppb = 2.00 $\mu g\,m^{-3}$) in order to stoichiometrilly compare OX and NO_x. The linear regressions obtained in the oxidant plot (Fig. 11b) show a regional day time contribution for the three urban sites (UB, RS and TCg) remarkably similar at 41–45 ppb (82–90 $\mu g\,m^{-3}$). The lower average values of 30 ppb (60 $\mu g\,m^{-3}$) for the regional contribution of the RB site may be due to enhanced regional deposition at the RB site and/or the urban heat island effect affecting the ozone concentrations at urban ground level (UB/RS/TCg sites).

The day time gradients of the OX-NO_x relationship shown in Fig. 11b are very different and increasing following the order RS (0.05), UB (0.13), TCg (0.34) and RB (1.5). As mentioned above, the gradient is thought to be indicative of local primary NO_2 emissions, or formation (with NO_x) of species which promote NO-to-NO_2 conversion, i.e. HO_2 and RO_2 radical precursors.

The variation in incoming ozone over the diurnal period (indicated by the intercept, Fig. 11c) shows a clear late morning/early afternoon maximum, peaking at 3 p.m., reflecting (modest) regional photochemical ozone production, common to all sites. More complex is the gradient, yet not fully understood. An increase in the gradient in the evening shows a stable night time atmosphere trapping NO_x, whereas a decline in the evening may reflect nitric acid formation via N_2O_5 and loss of NO_x by deposition or aerosol formation. NO effectively curtail the night time NO_3–N_2O_5 chemistry although Benton et al. (2010) found that the N_2O_5 formation above an urban city is significant. Despite its importance, many aspects of tropospheric N_2O_5 chemistry are still not well known. The rate of N_2O_5 uptake by particles – which depends on aerosol composition and meteorological conditions (RH and T) – remains highly uncertain (Brown et al., 2006; Chang et al., 2011). The impact of NO_3 chemistry on polluted atmospheres and urban air quality is, however, not well understood, due to a lack of observations and

Presenting SAPUSS

M. Dall'Osto et al.

the strong impact of vertical stability of the boundary layer, which makes nocturnal chemistry highly altitude dependent (Stutz et al., 2009; Harrison et al., 2012).

4.5 Aerosol size distribution, particle number and aerosol chemical concentrations

4.5.1 Aerosol size distributions

Aerosol number size distributions in the urban area are mainly a function of a number of factors, including primary emissions (i.e. traffic, power plants, cooking and heating), meteorological factors, and long-range transport of different sources of diverse regions (Hussain et al., 2006). Additionally, formation of new secondary particles in the urban atmosphere is most efficient when primary particle concentrations are low. Little is known about the vertical distribution of ultrafine particles in the urban atmosphere. The vertical extent of new aerosol particle formation is uncertain, with evidence for both new aerosol particle formation at the surface layer mixing upwards (O'Dowd et al., 2009) and nucleation occurring aloft and subsequently blended downwards (Siebert et al., 2004).

Figure 12 shows the average aerosol size distribution for 4 different sites (RS, UB, TC and RB). The RS site presents an aerosol size distribution typical for traffic conditions, with two fitted lognormal modes at 22 ± 1 nm and 47 ± 8 nm, respectively (Dall'Osto et al., 2011). A third accumulation mode is found at 125 ± 10 nm. The UB site shows a reduced nucleation mode at 14 ± 1 nm, whereas the Aiken (50 ± 2 nm) and the accumulation modes (122 ± 25 nm) are similar. At the TCg a similar smaller mode is fitted at 14 ± 3 nm, 40 ± 2 nm and 125 ± 130 nm. By contrast, at the RB site two larger Aitken modes (45 ± 5 nm and 70 ± 2 nm) and a third larger accumulation mode at 155 ± 5 nm are found. Future extensively analysis of aerosol size distributions obtained during SAPUSS will be carried out by using a novel application of cluster analysis (Beddows et al., 2009) and positive matrix factorization (Harrison et al., 2011).

4.5.2 Total particle number and black carbon concentrations

Total averaged particle number concentrations ($N_{>5-7}$) for the whole period of the SAPUSS study are presented in Table 5. The highest concentration of averaged particle number concentrations was found at the RS ($N_{>7}$: $12\,890 \pm 6300\,\mathrm{cm}^{-3}$), followed by UB ($N_{>5}$: $10\,490 \pm 5900\,\mathrm{cm}^{-3}$), TM ($N_{>7}$: $9590 \pm 6400\,\mathrm{cm}^{-3}$), TC ($N_{>7}$: $5500 \pm 3800\,\mathrm{cm}^{-3}$) and RB ($N_{>5}$: $2600 \pm 1800\,\mathrm{cm}^{-3}$) sites. A similar trend was seen for BC: the highest values for RS ($2990 \pm 1700\,\mathrm{ng\,m}^{-3}$), followed in the same order by UB ($1350 \pm 1100\,\mathrm{ng\,m}^{-3}$), TM ($1405 \pm 1500\,\mathrm{ng\,m}^{-3}$) and TC ($650 \pm 450\,\mathrm{ng\,m}^{-3}$). This is consistent with road traffic being a major source of both BC and N. The slightly higher value of BC at the TM site relative to UB is likely due to the busy highways and roads found below the TM site. The ratio between N and the more conservative variable BC (Dall'Osto et al., 2011) at the RS site was found constant at about 4 under different air mass conditions. By contrast, the other monitoring sites presented very different N/BC ratios under different air mass scenarios, implying different evolutions of particles leaving the main traffic source as well as contributions from primary and secondary particles from other sources.

Many studies have focused on the evolution of vehicular particles during advection away from the source, with very few studies focused on the vertical variations of particle number concentrations and size distributions. Whilst a more in depth analysis can be found elsewhere (Dall'Osto et al., 2012a, b), it is worth to report that one regional nucleation event was recorded simultaneously at all monitoring sites on the 25 September 2010 over the urban area of Barcelona, whereas a more confined urban nucleation event was detected on the 5 October 2010 with particles found to be growing (2–3$\,\mathrm{nm\,h}^{-1}$) later on in the background RB location while being transported away from the city. Finally, during non-nucleation event days, we found the highest N concentrations at the ground monitoring sites. By contrast, during nucleation days (characterized by high solar radiations and low RH) we found higher particle number above the city relative to the ground.

M. Dall'Osto et al.

Title Page

Abstract	Introduction
Conclusions	References
Tables	Figures

◀◀ ▶▶

◀ ▶

Back | Close

Full Screen / Esc

Printer-friendly Version

Interactive Discussion

4.5.3 Aerosol mass loadings averages

Table 6 shows the average PM_{10}, $PM_{2.5}$ and PM_1 concentrations measured both gravimetrically and by optical counters. Similar size fraction variations and inter-sites variations were observed for both the gravimetric and the optical data. For coherence and higher data coverage, only gravimetrically corrected optical data are herein discussed. The highest PM_{10} concentrations were recorded at the RS site (30.7 μg m^{-3}), followed by the UB (25.9 μg m^{-3}) and the TM (24.9 μg m^{-3}) urban sites. The lowest PM_{10} concentrations were recorded at background TC, TCg and RB sites, suggesting that the city surface is enhanced in coarse particles (Amato et al., 2009). By contrast, whilst the PM_1 showed the highest concentration also at the RS site (16.3 μg m^{-3}), the second highest concentrations were found at the tower sites (TM, TC) followed by the ground sites (TCg, UB, RB). This is better seen in the PM_1/PM_{10} ratios, showing the highest values of 0.59 and 0.73 at the TM and TC, respectively. These results are in line with a recent study conducted in London, showing higher concentrations of fine aerosol above the city, where the cooler temperatures and higher relative humidity may shift the gas/aerosol ammonium nitrate equilibrium towards the aerosol phase (Harrison et al., 2012). It is important to note that the high PM_1/PM_{10} ratios at the towers (TM, TC) are not only due to the low PM_{10} concentrations, as the absolute values of PM_1 detected at the tower sites were also higher than the urban background ground levels (UB, TCg, Table 6). $PM_{2.5}$ did not show any clear trend at the urban sites, with average values of 17 ± 2 μg m^{-3}; whereas at the RB site the $PM_{2.5}$ concentrations were significantly lower (10.9 μg m^{-3}). When comparing PM concentrations within each monitoring site (Table 7), expected high correlations were found between PM_1 and $PM_{2.5}$ (R^2 0.8–0.95) and between $PM_{2.5}$ and PM_{10} (R^2 0.7–0.9); whereas weaker ones between PM_1 and PM_{10} (R^2 0.5–0.6). When analysing the inter-site variability, excluding the RB site, PM_1 and $PM_{2.5}$ were found to be correlated (R^2 0.6 and 0.55, averaged by considering all sites, respectively) suggesting a regional distribution of the aerosols in the fine ranges. By contrast, PM_{10} presented lower average R^2 (0.3), suggesting a higher dependence

Full Screen / Esc

Printer-friendly Version

Interactive Discussion

on local sources. The two tower sites (TM, TC) did not show a strong correlation, indicating differences in the atmosphere above the city. Overall, the total average R^2 (average of R^2 of each size fraction with the same size fraction at the rest of the sites) were, in order: 0.23 (RB), 0.33 (RS), 0.43 (TC), 0.47 (TM), 0.52 (UB) and 0.62 (TCg).

This indicates that the RB site was, as expected, disconnected from the urban monitoring sites. The RS was strongly affected by the traffic local source, hence presenting low correlations with the rest of the monitoring sites, especially for the PM_{10} fraction, which was found not correlating with any other PM size fraction of any site.

The temporal variability of the PM is presented in Fig. 13a. It should be noticed that the highest concentrations of PM_1 were recorded between the 13 and the 18 October, concomitant with the regional aerosol pollution described in Sect. 4.1. In particular, levels of PM_1 were found to be enhanced in the TM site relative to the other sites, whereas the PM_{10} concentrations did not present such variation.

As regard of diurnal trends (Fig. 13b), PM_1 was found to vary little across the time of the day within the city centre, suggesting mainly a regional contribution and/or slow deposition, which maintains the particles constantly in the urban atmosphere although the emissions do vary throughout the day. By contrast, PM_1 concentrations at the RB site were clearly dependent on the sea breeze bringing pollution from the city during the afternoon. The PM_{10} diurnal variation was influenced by traffic rush hours at all urban sites (RS, UB, TM), with the highest day-night differences found at the RS, probably reflecting the higher influence of dust resuspension at the traffic site (Fig. 13b). As a case study, Fig. 13c shows two different scenarios: Regional conditions (Reg.: stagnant regional air masses without accumulation of nitrate containing aerosols, 29–30 September 2010) and Regional conditions with nitrate containing aerosols (Reg-Nit: stagnant regional air masses with accumulation of nitrate containing aerosols, 15–16 October 2010). In order to visually report the main difference within the urban area of Barcelona, Fig. 13c reports only three urban monitoring sites: the urban tower (TM), the road site (RS) and the urban background (UB). PM_{10} concentrations levels do not show a clear variation within the monitoring sites. By contrast, when the fine (PM_1) and

coarse (PM_{1-10}) fractions are separated, a sticking opposite trend can be seen in the vertical urban column: higher loadings of fine aerosol mass at the towel level (TM) but higher loadings of coarse aerosol mass at the ground levels (UB, RS).

Finally, some considerations should be made on the air quality limit values for PM_{10}

5 (daily limit of $50\,\mu g\,m^{-3}$) and $PM_{2.5}$ (year average of $25\,\mu g\,m^{-3}$) set by the first Daughter Directive to the Air Quality Framework Directive sets (EEA, 2010) and the Clean Air for Europe (CAFE) lead the European Parliament. During the 32 days of the SAPUSS field study, the PM_{10} daily limits were never exceeded in any of the monitoring site.

4.5.4 Chemical analysis at the SAPUSS monitoring sites

10 Table 8 reports average fine (PM_1), coarse (PM_{1-10}) and total PM_{10} (fine and coarse) chemical components concentrations measured during SAPUSS (standard IDAEA-CSIC filter analysis, see Sect. 3.2.2) and grouped as follow: sulfate (SO_4^{2-}), nitrate (NO_3^-), ammonium (NH_4^+), organic matter (OM), Elemental Carbon (EC), marine aerosols (sum of Na and Cl), crustal aerosols (sum of Al_2O_3, SiO_2, CO_3^{2-}, Ca, Fe, K,

15 Mg, Mn, Ti and P – see Querol et al., 2001b), and the unaccounted mass. Overall, the different monitoring sites presented different trends (Table 8). The main fine chemical component at the RS site was found to be OC, followed by sulphate and EC. By contrast, the coarse fraction was dominated by the crustal component. Relative to the average of other urban sites, this component presented a large increment (76%) at

20 the RS site, indicating road dust as a major source of PM in the road site environment. When the total (fine and coarse) PM_{10} fractions are considered, similar concentrations at the five monitoring sites for ammonium and sulphate can be seen, but higher levels of OC, EC and crustal aerosols were found at the RS. The two background sites (TCg, RB) presented overall similar concentrations for all different chemical compo-

25 nents. Interestingly, levels of nitrate were found at higher level at the TM and RS relative to the remaining three monitoring sites (UB, TCg and RB). Previous studies showed that the NH_3-HNO_3-NH_4NO_3 system is sufficiently dynamic to result in a considerable

variability of NH_4NO_3 at urban level. Measurements of nitrate aerosol with the ATOFMS showed two types of nitrate-rich particle with contrasting behaviors: nitrate regionally transported and nitrate formed locally (Dall'Osto et al., 2009). Additionally, the cooler temperatures and higher relative humidity on the tower level can shift the gas/aerosol equilibrium towards the aerosol phase (Harrison et al., 2012). Future SAPUSS receptor modelling studies will try to apportion the sources and the processes of nitrate occurring both horizontally and vertically in the Barcelona urban atmosphere.

A brief summary of the chemical analysis of the aerosols collected at the two SAPUSS supersites is also presented. The molecular organic tracers (see Sect. 3.2.2) were analyzed from PM_1 filters that were collected at the UB and RS stations at 12 h intervals from 22 September to 18 October 2010. Higher concentrations of primary organic compounds were observed at the RS site compared to UB one i.e.: polycyclic aromatic hydrocarbons (PAH) (1.79 ± 0.75 and $0.87 \pm 0.4\,\mathrm{ng\,m^{-3}}$, respectively), hopanes (1.49 ± 0.8 and $0.98 \pm 0.45\,\mathrm{ng\,m^{-3}}$, respectively), nicotine (59 ± 40 and $7 \pm 5\,\mathrm{ng\,m^{-3}}$, respectively) and cholesterol (1.4 ± 0.6 and $0.8 \pm 0.3\,\mathrm{ng\,m^{-3}}$, respectively). By contrast, other selected organic compounds were found at higher concentrations at the UB site compared to the RS one, including: levoglucosan, a molecular tracer for biomass burning (1.79 ± 0.75 and $0.87 \pm 0.4\,\mathrm{ng\,m^{-3}}$, respectively), and dicarboxylic acids, for example malic acid (14 ± 12 and $10 \pm 7\,\mathrm{ng\,m^{-3}}$, respectively), a tracer compounds for secondary organic aerosols.

The two ATOFMSs (see Sect. 3.2.1) deployed simultaneously during the SAPUSS successfully collected in real time 1 042 331 and 274 974 single particle mass spectra at the RS and UB, respectively. About twenty different particle types were classified by the Art-2a clustering algorithm – some of which were found simultaneously at the two sites. Specifically, a particle type internally mixed with elemental carbon and nitrate was found mainly during the last part of the SAPUSS campaign. NaCl-containing particles were highly enhanced during windy Atlantic air masses. A variety of particle types internally mixed with organic nitrogen (including amines) found at higher concentrations at the road site and spiking at both day and night time. The two HR-ToF-AMS (see

Presenting SAPUSS

M. Dall'Osto et al.

Title Page

Abstract	Introduction
Conclusions	References
Tables	Figures

|◄ | ►|

◄ | ►

Back | Close

Full Screen / Esc

Printer-friendly Version

Interactive Discussion

Sect. 3.2.1) recorded organic species as the most predominant one at both SAPUSS super sites (62 % and 54 % at the RS and UB, respectively). The second most abundant species was found to be sulphate, but it showed higher concentration at the UB site (19 % and 27 %, at RS and UB, respectively). Smaller proportions were found for nitrate (10 % and 6.7 %, at RS and UB, respectively) and ammonium (8 % and 11 %, at RS and UB, respectively), whereas chloride made a small contribution at both sites (< 1 %). PIXE analysis of the $PM_{2.5}$ streaker samples (see Sect. 3.2.2, and Dall'Osto et al., 2012c) allowed the assessment of hourly resolution elemental time trends of 17 elements (Na, Mg, Al, S, Cl, K, Ca, Ti, V, Cr, Mn, Fe, Ni, Cu, Zn, Sr, Pb). PMF was applied to the whole data set and nine factors were found at both supersites (in parenthesis the specific markers): regional sulphates (S); two industrial sources (one mainly with Zn-Mn from smelters and a second one with Pb-Cl from waste incinerators); non-exhaust traffic brake dust (Fe-Cu); biomass burning (K); aged marine aerosol (Na-Mg); Oil combustion (V-Ni); and two soil sources (Al-Ti mainly from Saharan dust and Ca from urban construction activity). Strong correlations among RS and UB sites for some of the nine different PM sources were found, particularly for regional sulphate, Saharan dust and industrial Pb-Cl ones. Finally, it was found that the three different dust sources (soil dust, urban dust and brake dust) make an important contribution on the total measured mass of the 17 elements, particularly the RS site (12 %, 6 % and 7 % of the total elements measured, respectively).

4.6 Modelling

The main goal of the results included here is not to provide a comprehensive evaluation of the model behavior for all the pollutants, but to highlight the ability of the modeling system MM5-EMEP-CHIMERE to reproduce PM_{10}, $PM_{2.5}$ and PM_1 levels during the SAPUSS field study when compared to measured concentrations of air pollutants in the different measuring points of the Barcelona Metropolitan Area. Figure 14 depicts the mean and 1-h maximum ground levels for these pollutants and Table 9 indicates the evaluation results. A number of metrics were used to examine the model

performance. The mean bias (B) is a common metric used to quantify the departure between modeled and observed quantities; meanwhile the mean normalized bias (MNB) represents a useful measure of the overall over- or under-estimation by the model. The model generally underestimates the SAPUSS average PM concentration observed in the Barcelona Metropolitan Area (B generally ranging from -1 to $-10\,\mu g\,m^{-3}$, with the largest biases appearing for PM_{10}; MNB from -5 to $-48\,\%$). The standard deviation, which provides an idea of the hourly variability of the measurements and simulations, (essential to characterize the amplitude of the daily cycles of pollutants) is also somehow underestimated by the simulations, especially for PM_1 except in the UB station. Hence, the measurements for SAPUSS will contribute to a better characterization of this intra-daily variability and to check why the amplitude of the daily cycle is not well captured generally by these models.

On the other hand, the results of the evaluation for PM_{10} (with lower biases compared to $PM_{2.5}$ and PM_1) indicate that the model performs accurately, taking into account that current CTM simulations underestimate the particulate matter concentrations by 30–50 %, using the current knowledge about aerosol physics and chemistry (Vautard et al., 2005), which is the order of magnitude found for SAPUSS modeling results. If the results of the evaluation are compared to the skill scores of recent works for several models (e.g. Vautard et al., 2009; Pay et al., 2010; Baldasano et al., 2011 and references therein), the MM5-EMEP-CHIMERE modeling system exhibits consistent scores for particulate matter (with mean values generally close to the observations-biases in the order of $-20\,\%$ to $-50\,\%$). Further studies with SAPUSS data will allow validating the aerosol composition and the ground levels of trace gases, needed for an accurate speciation of the emissions in the target area.

Table 9 also shows that errors for PM_{10} decrease following the direction coastline-inland. For instance, the MNB at the TM site, located by the coast, is around $-39\,\%$; this MNB decreases to $-27\,\%$ at the UB site and up to 5 % at the TC site. Overall, PM_{10} is less underestimated than $PM_{2.5}$ and PM_1, especially in TC and TCg. Largest biases for PM_{10} are found at RB. This negative bias may be produced by an underestimation in

Presenting SAPUSS

M. Dall'Osto et al.

the transport pattern. The high local contribution and the lack of transport of particulate matter are associated to the short lifetime of this kind of particles in the atmosphere of CTMs as a consequence of the fast deposition implemented (Jiménez-Guerrero et al., 2011b). In this same sense, Ellemann and Covert (2009) report an over-prediction of geometric mean diameter by CTMs and that aerosol size distributions are shifted to a larger size compared with observations (and that is likely the reason why PM_{10} is generally less underestimated than $PM_{2.5}$ and PM_1). This fact may affect the fine particulate matter predictions, which will increase if over-predictions of the geometric mean diameter are corrected. The information obtained from SAPUSS field measurements may play an important role for improving low-diameter particulate matter modeling results in the target area.

Moreover, the inaccuracies in representing accumulation and transport patterns during this period of simulation covering SAPUSS field campaign could be the origin of these underpredictions. Some emission sources are also missing in the emission model, such as the re-suspension from soils and paved roads in urban areas (Lenschow et al., 2001; Pay et al., 2011), which may exert a limited influence in the particulate matter levels in the area especially during the peak traffic hours. The underestimation of particulate matter levels (mainly in the case of PM_1) may be caused because of the average volume defined by the model horizontal grid spacing, that must be sufficiently small to allow the air quality to be reproduced accurately, especially on urban scales (Jiménez-Guerrero et al., 2008). It appears that a finer grid is important for addressing air pollution processes in urban areas, whereas for rural areas larger grids may be allowed, for example, to capture the non-linearity of the chemical formation as a function of precursor concentrations.

In summary, Fig. 14 shows that the complex topography of the Barcelona urban area (the Llobregat Valley on the left, the Besos Valley on the right and the Collserola hills on the top, Fig. 1a) does not allow a uniform dispersion of the atmospheric pollutants. Future SAPUSS-related modelling works will deal with a number of studies, such as meteorological validation of the integrations, an improvement of the vertical distribution

Presenting SAPUSS

M. Dall'Osto et al.

CC BY

of aerosols and the dynamical transport of the model, assessment of the chemical composition of aerosol (focusing in the inclusion of new aerosols, such as BC), validation of both the mass and the particle number in different measurement points, etc. SAPUSS constitutes a valuable database for modellers to understand the processes
5 behind the biases and typical errors of chemistry transport models.

5 Conclusions

Air pollution is a priority field in today's environmental research. Health effects associated with air pollution exposure drives air quality regulations worldwide. Most of the air quality problems stem from continued growth in population, heavy industry, and vehicle
10 traffic. Additionally, complex area topography and climatology play also an important rule. The complex physical and chemical properties of air pollution require an array of instruments to try to cover the full picture of the source identification of air pollutants in the atmosphere. SAPUSS laid the foundation for providing relevant results to allow the identification of emission sources and their respective contribution to the air pollu-
15 tants in ambient air of an urban Mediterranean coastal environment (Barcelona). This paper presents an overview of the six monitoring sites used during the SAPUSS: traffic hot spot road site (RS), two urban background sites (UB and TCg), two towers sites (TM and TC) and a regional background site (RB). During the four weeks intensive field study a number of different air masses were encountered: continental and ma-
20 rine polar and continental and marine tropical. Both the spatial vertical and horizontal distributions of air pollutants were investigated to better understand the complex interactions between these pollutants and different meteorological variables, as well as their influence on air quality. Boundary layer analysis coupled with local meteorology and gaseous pollutants measurements revealed stratification of pollutants above the
25 city. High levels of traffic gaseous pollutants were measured at the urban ground monitoring sites, whereas layers of tropospheric ozone were recorded at tower levels. BC, N and mass concentrations (PM_x) measured simultaneously in three spatial dimensions

Presenting SAPUSS

M. Dall'Osto et al.

showed a complex relationship between traffic related particles and urban and regional nucleation events. All the results shown in this study – as well as the ones contained in this ACP SAPUSS special issue – will be modelled, in an attempt to reduce the need for fixed continuous monitoring sites, and also coverage of a wider urban area rather than a specific location where a monitoring site is located. More information on the SAPUSS measurements and their analysis can be found in this special issue.

References

Amato, F., Pandolfi, M., Viana, M., Querol, X., Alastuey, A., and Moreno, T.: Spatial and chemical patterns of PM_{10} in road dust deposited in urban environment, Atmos. Environ., 43, 1650–1659, 2009.

Baldasano, J. M., Pay, M. T., Jorba, O., Gassó, S., and Jiménez-Guerrero, P.: An annual assessment of air quality with the CALIOPE modeling system over Spain, Sci. Total Environ., 409, 2163–2178, doi:10.1016/j.scitotenv.2011.01.041, 2011.

Beddows, D. C. S., Dall'Osto, M., and Harrison, R. M.: Cluster analysis of rural, urban and curbside atmospheric particle size data, Environ. Sci. Technol., 43, 4694–4700, 2009.

Benton, A. K., Langridge, J. M., Ball, S. M., Bloss, W. J., Dall'Osto, M., Nemitz, E., Harrison, R. M., and Jones, R. L.: Night-time chemistry above London: measurements of NO_3

◀◀ | ▶▶

◀ | ▶

Back | Close

Full Screen / Esc

Printer-friendly Version

Interactive Discussion

and N$_2$O$_5$ from the BT Tower, Atmos. Chem. Phys., 10, 9781–9795, doi:10.5194/acp-10-9781-2010, 2010.

Bessagnet, B., Hodzic, A., Vautard, R., Beekmann, M., Cheinet, S., Honore, C., Liousse, C., and Rouil, L.: Aerosol modeling with CHIMERE – preliminary evaluation at the continental scale, Atmos. Environ., 38, 2803–2817, 2004.

Birch, M. E. and Cary, R. A.: Elemental carbon-based method for monitoring occupational exposures to particulate diesel exhaust, Aerosol. Sci. Tech., 25, 221–241, 1996.

Brown, S. S., Ryerson, T. B., Wollny, A. G., Brock, C. A., Peltier, R., Sullivan, A. P., Weber, R. J., Dube, W. P., Trainer, M., Meagher, J. F., Fehsenfeld, F. C., and Ravishankara, A. R.: Variability in nocturnal nitrogen oxide processing and its role in regional air quality, Science, 311, 67–70, 2006.

Canagaratna, M. R., Jayne, J. T., Jimenez, J. L., Allan, J. D., Alfarra, M. R., Zhang, Q., Onasch, T. B., Drewnick, F., Coe, H., Middlebrook, A., Delia, A., Williams, L. R., Trimborn, A. M., Northway, M. J., DeCarlo, P. F., Kolb, C. E., Davidovits, P., and Worsnop, D. R.: Chemical and microphysical characterization of ambient aerosols with the aerodyne aerosol mass spectrometer, Mass Spectrom. Rev., 26, 185–222, 2007.

Cavalli, F., Viana, M., Yttri, K. E., Genberg, J., and Putaud, J.-P.: Toward a standardised thermal-optical protocol for measuring atmospheric organic and elemental carbon: the EUSAAR protocol, Atmos. Meas. Tech., 3, 79–89, doi:10.5194/amt-3-79-2010, 2010.

Chang, W., Bhave, P., Brown, S., Riemer, N., Stutz, J., and Dabdub, D.: Tropospheric N$_2$O$_5$: a review of ambient measurements and model calculations, Aerosol Sci. Technol., 45, 655–685, 2011.

Chiari, M., Lucarelli, F., Mazzei, F., Nava, S., Paperetti, L., Prati, P., Valli, G., and Vecchi, R.: Characterization of airborne particulate matter in an industrial district near Florence by PIXE and PESA, X-Ray Spectrom., 34, 323–329, 2005.

Clapp, L. J. and Jenkin, M. E.: Analysis of the relationship between ambient levels of O$_3$, NO$_2$ and NO as a function of NO$_x$ in the UK, Atmos. Environ., 35, 6391–6405, 2001.

Dall'Osto, M., Harrison, R. M., Beddows, D. C. S., Freney, E. J., Heal, M. R., and Donovan, R. J.: Single particle detection efficiencies of aerosol time of flight mass spectrometry during the North Atlantic marine boundary layer experiment, Environ. Sci. Technol., 40, 5029–5035, doi:10.1021/es050951i, 2006.

Title Page

Abstract	Introduction
Conclusions	References
Tables	Figures

◀◀ ▶▶

◀ ▶

Back Close

Full Screen / Esc

Printer-friendly Version

Interactive Discussion

Dall'Osto, M., Harrison, R. M., Coe, H., Williams, P. I., and Allan, J. D.: Real time chemical characterization of local and regional nitrate aerosols, Atmos. Chem. Phys., 9, 3709–3720, doi:10.5194/acp-9-3709-2009, 2009.

Dall'Osto, M., Thorpe, A., Beddows, D. C. S., Harrison, R. M., Barlow, J. F., Dunbar, T., Williams, P. I., and Coe, H.: Remarkable dynamics of nanoparticles in the urban atmosphere, Atmos. Chem. Phys., 11, 6623–6637, doi:10.5194/acp-11-6623-2011, 2011.

Dall'Osto, M., Beddows, D. C. S., Pey, J., Rodriguez, S., Alastuey, A., Harrison, R. M., and Querol, X.: Urban aerosol size distributions over the Mediterranean city of Barcelona, NE Spain, Atmos. Chem. Phys. Discuss., 12, 16457–16492, doi:10.5194/acpd-12-16457-2012, 2012a.

Dall'Osto, M., Querol, X., Alastuey, A., O'Dowd, C., Harrison, R. M., Wenger, J., and Gòmez-Moreno, F. J.: On the spatial distribution and evolution of ultrafine aerosols in urban air, Atmos. Chem. Phys. Discuss., 12, 16603–16646, doi:10.5194/acpd-12-16603-2012, 2012b.

Dall'Osto, M., Querol, X., Amato, F., Karanasiou, A., Lucarelli, F., Nava, S., Calzolai, G., and Chiari, M.: Hourly elemental concentrations in $PM_{2.5}$ aerosols sampled simultaneously at urban background and road site, Atmos. Chem. Phys., SAPUSS special issue, submitted, 2012c.

DeCarlo, P. F., Kimmel, J. R., Trimborn, A., Northway, M. J., Jayne, J. T., Aiken, A. C., Gonin, M., Fuhrer, K., Horvath, T., Docherty, K. S., Worsnop, D. R., and Jimenez, J. L.: Field-deployable, high-resolution, time-of-flight aerosol mass spectrometer, Anal. Chem., 78, 8281–8289, 2006.

de Foy, B., Varela, J. R., Molina, L. T., and Molina, M. J.: Rapid ventilation of the Mexico City basin and regional fate of the urban plume, Atmos. Chem. Phys., 6, 2321–2335, doi:10.5194/acp-6-2321-2006, 2006.

Derognat, C., Beekmann, M., Baeumle, M., Martin, D., and Schmidt, H.: Effect of biogenic volatile organic compound emissions on tropospheric chemistry during the Atmospheric Pollution over the Paris Area (ESQUIF) campaign in the Ile-de-France region, J. Geophys. Res., 108, 8560, doi:10.1029/2001JD001421, 2003.

Díaz-de-Quijano, M., Peñuelas, J., and Ribas, A.: Increasing interannual and altitudinal ozone mixing ratios in the Catalan Pyrenees, Atmos. Environ., 43, 6049–6057, 2009.

Draxler, R. R. and Rolph, G. D.: Hysplit (hybrid single-particle lagrangian integrated trajectory) model (http://www.Arl.Noaa.Gov/ready/hysplit4.html (last access: July 2012), NOAA Air Resources Laboratory, Silver Spring, MD, USA, 2003.

Title Page

Abstract | Introduction

Conclusions | References

Tables | Figures

◀ | ▶

◀ | ▶

Back | Close

Full Screen / Esc

Printer-friendly Version

Interactive Discussion

Dudhia, J.: A nonhydrostatic version of the Penn State NCAR mesoscale model: validation tests and simulation of an Atlantic cyclone and cold front, Mon. Weather Rev., 121, 1493–1513, 1993.

EEA: Reporting on Ambient Air Quality Assessment in the EU Member States, 2008ETC/ACC Technical Paper 2010/11, December 2010.

Elleman, R. A. and Covert, D. S.: Aerosol size distribution modeling with the Community Multi-scale Air Quality modeling system (CMAQ) in the Pacific Northwest: 1. model comparison to observations, J. Geophys. Res., 114, D11206, doi:10.1029/2008JD010791, 2009.

Escudero, M., Castillo, S., Querol, X., Avila, A., Alarcón, M., Viana, M. M., Alastuey, A., Cuevas, E., and Rodríguez, S.: Wet and dry African dust episodes over Eastern Spain, J. Geophys. Res., 110, 4731–4746, 2005.

Formenti, P., Prati, P., Zucchiatti, A., Lucarelli, F., and Mandó, P. A.: Aerosol study in the town of Genova with a PIXE analysis, Nucl. Instrum. Methods, 113, 359–362, 1996.

Gard, E., Mayer, J. E., Morrical, B. D., Dienes, T., Fergenson, D. P., and Prather, K. A.: Real-time analysis of individual atmospheric aerosol particles: design and performance of a portable ATOFMS, Anal. Chem., 69, 4083–4091, 1997.

Grell, A. G., Dudhia, J., and Stauffer, D. R.: A description of the fifth-generation PennState/NCAR mesoscale model (MM5), NCAR Technical Note NCAR/TN-398+STR, Natl. Cent. Atmos. Res., Boulder, CO, 138 pp., 1994.

Gross, D. S., Galli, M. E., Silva, P. J., and Prather, K. A.: Relative sensitivity factors for alkali metal and ammonium cations in single particle aerosol time-of-flight mass spectra, Anal. Chem., 72, 416–422, 2000.

Gong, L., Lewicki, R., Griffin, R. J., Flynn, J. H., Lefer, B. L., and Tittel, F. K.: Atmospheric ammonia measurements in Houston, TX using an external-cavity quantum cascade laser-based sensor, Atmos. Chem. Phys., 11, 9721–9733, doi:10.5194/acp-11-9721-2011, 2011.

Haeffelin, M., Angelini, F., Morille, Y., Martucci, G., O'Dowd, C. D., Xueref-Rémy, I., Wastine, B., Frey, S., and Sauvage, L.: Evaluation of mixing depth retrievals from automatic profiling lidars and ceilometers in view of future integrated networks in Europe, Bound.-Lay. Meteorol., doi:10.1007/s10546-011-9643-z, 2011.

Heese, B., Flentje, H., Althausen, D., Ansmann, A., and Frey, S.: Ceilometer lidar comparison: backscatter coefficient retrieval and signal-to-noise ratio determination, Atmos. Meas. Tech., 3, 1763–1770, doi:10.5194/amt-3-1763-2010, 2010.

Presenting SAPUSS

M. Dall'Osto et al.

Title Page

Abstract	Introduction
Conclusions	References
Tables	Figures

◀ | ▶

◀ | ▶

Back | Close

Full Screen / Esc

Printer-friendly Version

Interactive Discussion

Harrison, R. M., Beddows, D. C. S., and Dall'Osto, M.: PMF analysis of wide-range particle size spectra collected on a major highway environ, Environ. Sci. Technol., 45, 5522–5528, doi:10.1021/es2006622, 2011.

Harrison, R. M., Dall'Osto, M., Beddows, D. C. S., Thorpe, A. J., Bloss, W. J., Allan, J. D.,
Coe, H., Dorsey, J. R., Gallagher, M., Martin, C., Whitehead, J., Williams, P. I., Jones, R. L., Langridge, J. M., Benton, A. K., Ball, S. M., Langford, B., Hewitt, C. N., Davison, B., Martin, D., Petersson, K. F., Henshaw, S. J., White, I. R., Shallcross, D. E., Barlow, J. F., Dunbar, T., Davies, F., Nemitz, E., Phillips, G. J., Helfter, C., Di Marco, C. F., and Smith, S.: Atmospheric chemistry and physics in the atmosphere of a developed megacity (London): an overview
of the REPARTEE experiment and its conclusions, Atmos. Chem. Phys., 12, 3065–3114, doi:10.5194/acp-12-3065-2012, 2012.

Hussein, T., Karppinen, A., Kukkonen, J., Härkönen, J., Aalto, P. P., Hämeri, K., Kerminen. V.-M., and Kulmala, M.: Meteorological dependence of size-fractioned number concentrations of urban aerosol particles, Atmos. Environ., 40, 1427–1440, 2006.

IPCC: Climate Change 2007: The Physical Science Basis. Contribution of Working Group I to the Fourth Assessment Report of the Intergovernmental Panel on Climate Change, edited by: Solomon, S., Qin, D., Manning, M., Chen, Z., Marquis, M., Averyt, K. B., Tignor , M., and Miller , H. L., Cambridge University Press, Cambridge, UK and New York, NY, USA, 996 pp., 2007.

Jayne, J. T., Leard, D. C., Zhang, X. F., Davidovits, P., Smith, K. A., Kolb , C. E., and Worsnop, D. R.: Development of an aerosol mass spectrometer for size and composition analysis of submicron particles, Aerosol Sci. Tech., 33, 49–70, 2000.

Jimenez, P., Lelieveld, J., and Baldasano, J. M.: Multiscale modeling of air pollutants dynamics in the Northwestern Mediterranean basin during a typical summertime episode, J. Geophys. Res., 111, D18306, doi:10.1029/2005JD006516, 2006.

Jiménez-Guerrero, P., Jorba, O., Baldasano, J. M., Gassó, S.: The use of a modelling system as a tool for air quality management: annual high-resolution simulations and evaluation, Sci. Total Environ., 390, 323–340, doi:10.1016/j.scitotenv.2007.10.025, 2008.

Jiménez-Guerrero, P., Gómez-Navarro, J. J., Jerez, S., Lorente-Plazas, R., García Valero, J. A., and Montávez, J. P.: Isolating the effects of climate change in the variation of secondary inorganic aerosols (SIA) in Europe for the 21st century (1991–2100), Atmos. Environ., 45, 1059–1063, doi:10.1016/j.atmosenv.2010.11.022, 2011a.

Jiménez-Guerrero, P., Jorba, O., Pay, M. T., Montávez, J. P., Jerez, S., Gómez-Navarro, J. J., and Baldasano, J. M.: Comparison of two different sea-salt aerosol schemes as implemented in air quality models applied to the Mediterranean Basin, Atmos. Chem. Phys., 11, 4833–4850, doi:10.5194/acp-11-4833-2011, 2011b.

5 Jorba, O., Perez, C., Rocadenbosch, F., and Baldasano, J.: Cluster analysis of 4-day back trajectories arriving in the Barcelona area (Spain) from 1997 to 2002, J. Appl. Meteorol., 43, 887–901, 2004.

Kanakidou, M., Mihalopoulos, N., Kindap, T., Im, U., Vrekoussis, M., Gerasopoulos, E., Dermitzaki, E., Unal, A., Kocak, M., Markakis, K., Melas, D., Kouvarakis, G., Youssef, A. F.,

10 Richter, A., Hatzianastassiou, N., Hilboll, A., Ebojie, F., Wittrock F, von Savigny, C., and Burrows, J. P.: Megacities as hot spots of air pollution in the East Mediterranean, Atmos. Environ., 45, 1223–1235, 2011.

Koçak, M., Mihalopoulos, N., and Kubilay, N.: Contributions of natural sources to high PM_{10} and $PM_{2.5}$ events in the Eastern Mediterranean, Atmos. Environ., 41, 3806–3818, 2008.

15 Lenschow, P., Abraham, H. J., Kutzner, K., Lutz, M., Preu, J. D., and Reichenbcher, W.: Some ideas about the sources of PM_{10}, Atmos. Environ., 35, Supplement No. 1, S23, 2011.

Martucci, G., Milroy, C., and O'Dowd, C. D.: Detection of cloud base height using Jenoptik CHM15K and Vaisala CL31 ceilometers, J. Atmos. Ocean. Tech., 27, 305–318, 2010.

Maxwell, J. A., Teesdale, W. J., and Campbell, J. L.: The Guelph PIXE package II, Nucl. Instrum.
20 Methods, 95, 407–21, 1995.

McMurry, P. H.: A review of atmospheric aerosol measurements, Atmos. Environ., 34, 1959–1999, 2000.

Meng, Z. Y., Lin, W. L., Jiang, X. M., Yan, P., Wang, Y., Zhang, Y. M., Jia, X. F., and Yu, X. L.: Characteristics of atmospheric ammonia over Beijing, China, Atmos. Chem. Phys., 11, 6139–
25 6151, doi:10.5194/acp-11-6139-2011, 2011.

Millan, M. M., Salvador, R., Mantilla, E., and Kallos, G.: Photo-oxidant dynamics in the Mediterranean Basin in summer: results from European research projects, J. Geophys. Res., 102, 8811–8823, doi:10.1029/96JD03610, 1997.

Millan, M. M., Mantilla, E., Salvador, R., Carratalá, A., Sanz, M. J., Alonso, L., Gangoiti, G., and
30 Navazo, M.: Ozone cycles in the Western Mediterranean basin: interpretation of monitoring data in complex coastal terrain, J. Appl. Meteorol., 39, 487–508, 73–83, 2000.

Minguillón, M. C., Perron, N., Querol, X., Szidat, S., Fahrni, S. M., Alastuey, A., Jimenez, J. L., Mohr, C., Ortega, A. M., Day, D. A., Lanz, V. A., Wacker, L., Reche, C., Cusack, M., Amato, F.,

Kiss, G., Hoffer, A., Decesari, S., Moretti, F., Hillamo, R., Teinilä, K., Seco, R., Peñuelas, J., Metzger, A., Schallhart, S., Müller, M., Hansel, A., Burkhart, J. F., Baltensperger, U., and Prévôt, A. S. H.: Fossil versus contemporary sources of fine elemental and organic carbonaceous particulate matter during the DAURE campaign in Northeast Spain, Atmos. Chem. Phys., 11, 12067–12084, doi:10.5194/acp-11-12067-2011, 2011.

Mohr, C., DeCarlo, P. F., Heringa, M. F., Chirico, R., Slowik, J. G., Richter, R., Reche, C., Alastuey, A., Querol, X., Seco, R., Peñuelas, J., Jiménez, J. L., Crippa, M., Zimmermann, R., Baltensperger, U., and Prévôt, A. S. H.: Identification and quantification of organic aerosol from cooking and other sources in Barcelona using aerosol mass spectrometer data, Atmos. Chem. Phys., 12, 1649–1665, doi:10.5194/acp-12-1649-2012, 2012.

Nenes, A., Pandis, S. N., and Pilinis, C.: ISORROPIA: a new thermodynamic equilibrium model for multiphase multicomponent inorganic aerosols, Aquat. Geochem., 4, 123–152, 1998.

O'Dowd, C. D., Yoon, Y. J., Junkermann, W., Aalto, P., Kulmala, M., Lihavainen, H., and Viisanen, Y.: Airborne measurements of nucleation mode particles II: boreal forest nucleation events, Atmos. Chem. Phys., 9, 937–944, doi:10.5194/acp-9-937-2009, 2009.

Pay, M. T., Piot, M., Jorba, O., Gassó, S., Gonçalves, M., Basart, S., Dabdub, D., Jiménez-Guerrero, P., and Baldasano, J. M.: A full year evaluation of the CALIOPE-EU air quality modeling system over Europe for 2004, Atmos. Environ., 44, 3322–3342, doi:10.1016/j.atmosenv.2010.05.040, 2010.

Pay, M. T., Jiménez-Guerrero, P., and Baldasano, J.: Implementation of resuspension from paved roads for the improvement of CALIOPE air quality system in Spain, Atmos. Environ., 45, 802–807, 2011.

Pérez, C., Sicard, M., Jorba, O., Comeron, A., and Baldasano, J. M.: Summertime re-recirculations of air pollutants over the North-Eastern Iberian coast observed from systematic EARLINET lidar measurements in Barcelona, Atmos. Environ., 38, 3983–4000, 2004.

Pereza, C., Jimeneza, P., Jorbaa, O., Sicardb, M., and Baldasano, J. M.: Influence of the PBL scheme on highresolution photochemical simulations in an urban coastal area over the Western Mediterranean, Atmos. Environ., 40, 5274–5297, 2006.

Pey, J., Alastuey , A., and Querol, X.: Discriminating the regional and urban contributions in the North-Western Mediterranean: PM levels and composition, Atmos. Environ., 44, 1587–1596, 2010.

Pope, C. A. and Dockery, D. W.: Health effects of fine particulate air pollution: lines that connect, J. Air Waste Manage., 56, 709–742, 2006.

Presenting SAPUSS

M. Dall'Osto et al.

Title Page

Abstract	Introduction
Conclusions	References
Tables	Figures

|◄ | ►|

◄ | ►

Back | Close

Full Screen / Esc

Printer-friendly Version

Interactive Discussion

Pratt, K. A. and Prather, K. A.: Mass spectrometry of atmospheric aerosols – recent developments and applications. Part I: Off-line mass spectrometry techniques, Mass Spectrom. Rev., 31, 1–16, doi:10.1002/mas.20322, 2011a.

Pratt, K. A. and Prather, K. A.: Mass spectrometry of atmospheric aerosols – recent developments and applications. Part II: On-line mass spectrometry techniques, Mass Spectrom. Rev., 31, 17–48, doi:10.1002/mas.20330, 2011b.

Qin, X., Bhave, P. V., and Prather, K. A.: Comparison of two methods for obtaining quantitative mass concentrations from aerosol time-of-flight mass spectrometry measurements, Anal. Chem., 78, 6169–6178, 2006.

Querol, X., Alastuey, A., Puicercus, J. A., Mantilla, E., Miroa, J. V., Lopez-Soler, A., Plana, F., and Artinano, B.: Seasonal evolution of suspended particles around a large coal-fired power station: particulate levels and sources, Atmos. Environ., 32, 1963–1978, 1998.

Querol, X., Alastuey, A., Rodriguez, S., Plana, F., Ruiz, C. R., Cots, N., Massague, G., and Puig, O.: PM_{10} and $PM_{2.5}$ source apportionment in the Barcelona metropolitan area, Catalonia, Spain, Atmos. Environ., 35, 6407–6419, 2001a.

Querol, X., Alastuey, A., Rodriguez, S., Plana, F., Mantilla, E., and Ruiz, C. R.: Monitoring of PM_{10} and $PM_{2.5}$ around primary particulate anthropogenic emission sources, Atmos. Environ., 35, 845–858, 2001b.

Querol, X., Alastuey, A., Ruiz, C. R., Artinano, B., Hansson, H. C., Harrison, R. M., Buringh, E., Brink, H. M. T., Lutz, M., Bruckmann, P., Straehl, P., and Schneider, J.: Speciation and origin of PM_{10} and $PM_{2.5}$ in selected European cities, Atmos. Environ., 38, 6547–6555, 2004.

Querol, X., Pey, J., Pandolfi, M., Alastuey, A., Cusack, M., Perez, N., Moreno, T., Viana, M., Mihalopoulos, N., Kallos, G., and Kleanthous, S.: African dust contributions to mean ambient PM_{10} mass-levels across the Mediterranean Basin, Atmos. Environ., 43, 4266–4277, 2009.

Reche, C., Querol, X., Alastuey, A., Viana, M., Pey, J., Moreno, T., Rodríguez, S., González, Y., Fernández-Camacho, R., de la Rosa, J., Dall'Osto, M., Prévôt, A. S. H., Hueglin, C., Harrison, R. M., and Quincey, P.: New considerations for PM, Black Carbon and particle number concentration for air quality monitoring across different European cities, Atmos. Chem. Phys., 11, 6207–6227, doi:10.5194/acp-11-6207-2011, 2011.

Reche, C., Viana, M., Pandolfi, M., Alastuey, A., Moreno, T., Amato, F., Ripoll, A., and Querol, X.: Urban NH_3 levels and sources in a mediterranean environment, Atmos. Environ., 57, 153–164, 2012.

Presenting SAPUSS

M. Dall'Osto et al.

Rodríguez, S., Querol, X., Alastuey, A., and Mantilla, E.: Origin of high summer PM_{10} and TSP concentrations at rural sites in Eastern Spain, Atmos. Environ., 36, 3101–3112, 2002.

Rodríguez, S., Querol, X., Alastuey, A., Viana, M. M., and Mantilla, E.: Events affecting levels and seasonal evolution of airborne particulate matter concentrations in the Western Mediterranean, Environ. Sci. Technol., 37, 216–222, doi:10.1021/es020106p, 2003.

Rouil, L., Honore, C., Vautard, R., Beekmann, M., Bessagnet, B., Malherbe, L., Meleux, F., Dufour, A., Elichegaray, C., Flaud J-M, Menut, L., Martin, D., Peuch, A., Peuch, V.-H., and Poisson, N.: PREV'AIR, an operational forecasting and mapping system for air quality in Europe, B. Am. Meteorol. Soc., 90, 73–83, 2009.

Schmidt, H., Derognet, C., Vautard, R., and Beekmann, M.: A comparison of simulated and observed ozone mixing rations for the summer of 1998 in Western Europe, Atmos. Environ., 35, 6277–6297, 2001.

Seinfeld, J. H. and Pandis, S. N.: Atmospheric Chemistry and Physics. From Air Pollution to Climate Change, Wiley, New York, 1998.

Sicard, M., Rocadenbosch, F., Reba, M. N. M., Comerón, A., Tomás, S., García-Vízcaino, D., Batet, O., Barrios, R., Kumar, D., and Baldasano, J. M.: Seasonal variability of aerosol optical properties observed by means of a Raman lidar at an EARLINET site over Northeastern Spain, Atmos. Chem. Phys., 11, 175–190, doi:10.5194/acp-11-175-2011, 2011.

Siebert, H., Stratmann, F., and Wehner, B.: First observations of increased ultrafine particle number concentrations near the inversion of a continental planetary boundary layer and its relation to ground-based measurements, Geophys. Res. Lett., 31, L09102, doi:10.1029/2003GL019086, 2004.

Soriano, C., Baldasano, J. M., Buttler, W. T., and Moore, K.: Circulatory patterns of air pollutants within the Barcelona air basin in a summertime situation: lidar and numerical approaches, Bound.-Lay. Meteorol., 98, 33–55, 2001.

Stanier, C. O., Khlystov, A. Y., and Pandis, S. N.: Nucleation events during the Pittsburgh air quality study: description and relation to key meteorological, gas phase and aerosol parameters, Aerosol Sci. Tech., 38, 253–264, 2004.

Stutz, J., Wong, K. W., Lawrence, L., Ziemba, L., Flynn, J. H., Rappenglück, B., and Lefer, B.: Nocturnal NO_3 radical chemistry in Houston, TX, Atmos. Environ., 44, 4099, doi:10.1016/j.atmosenv.2009.03.004, 2009.

Su, Y. X., Sipin, M. F., Furutani, H., and Prather, K. A.: Development and characterization of an aerosol time-of-flight mass spectrometer with increased detection efficiency, Anal. Chem., 76, 712–719, 2004.

Suess, D. T. and Prather, K. A.: Mass spectrometry of aerosols, Chem. Rev., 99, 3007–3035, 1999.

Toll, I., and Baldasano, J. M.: Modeling of photochemical air pollution in the Barcelona area with highly disaggregated anthropogenic and biogenic emissions, Atmos. Environ., 34, 3060–3084, 2001.

Tang, Y. S., Cape, J. N., and Sutton, M. A.: Development and types of passive samplers for monitoring atmospheric NO_2 and NH_3 concentrations, The Scientific World, 1, 513–529, 2001.

Tong, N. Y. O., Leung, D. Y. C., and Liu, C.-H.: A review on ozone evolution and its relationship with boundary layer characteristics in urban environments, Water Air Soil Poll., 214, 13–36, 2011.

Vautard, R., Bessagnet, B., Chin, M., and Menut, L.: On the contribution of natural aeolian sources to particulate matter concentrations in Europe: testing hypotheses with a modelling approach, Atmos. Environ., 39, 3291–3303, doi:10.1016/j.atmosenv.2005.01.051, 2005.

Vautard, R., Schaap, M., Bergström, R., Bessagnet, B., Brandt, J., Builtjes, P. J. H., Christensen, J. H., Cuvelier, C., Foltescu, V., Graff, A., Kerschbaumer, A., Krol, M., Roberts, P., Rouïl, L., Stern, R., Tarrason, L., Thunis, P., Vignati, E., Wind, P.: Skill and uncertainty of a regional air quality model ensemble, Atmos. Environ., 43, 4822–4832, doi:10.1016/j.atmosenv.2008.09.083, 2009.

Vestreng, V., Myhre, G., Fagerli, H., Reis, S., and Tarrasón, L.: Twenty-five years of continuous sulphur dioxide emission reduction in Europe, Atmos. Chem. Phys., 7, 3663–3681, doi:10.5194/acp-7-3663-2007, 2007.

Viana, M., López, J. M., Querol, X., Alastuey, A., García-Gacio, D., Blanco-Heras, G., López-Mahía, P., Piñeiro- Iglesias, M., Sanz, M. J., Sanz, F., Chi, X., and Maenhaut, W.: Tracers and impact of open burning of rice straw residues on PM in Eastern Spain, Atmos. Environ., 42, 1941–1957, 2008.

Wong, K. W. and Stutz, J.: Influence of nocturnal vertical stability on daytime chemistry: a one-dimensional model study, Atmos. Environ., 44, 3753–3760, doi:10.1016/j.atmosenv.2010.06.057, 2010.

Presenting SAPUSS

M. Dall'Osto et al.

Title Page

Abstract | Introduction

Conclusions | References

Tables | Figures

◄ | ►

◄ | ►

Back | Close

Full Screen / Esc

Printer-friendly Version

Interactive Discussion

Table 1. Institutions taking part to SAPUSS.

	Institution	Country	Involvement
1	Institute of Environmental Assessment and Water Research (IDÆA), CSIC	ES	Project PI, on line and off line sampling collection and analysis of atmospheric pollutants
2	Division of Environmental Health and Risk Management, University of Birmingham	UK	ATOFMS, CPC, MOUDI
3	School of Physics and Centre for Climate and Air Pollution Studies, University of Galway	IR	Ceilometer, AMS
4	Aerodyne Inc	USA	AMS
5	Centre for Research into Atmospheric Chemistry, University of Cork	IR	ATOFMS
6	Department of Physics and Astronomy, University of Florence	IT	PIXE
7	Dept. of Chem. and Biochem. and CIRES Fellow, University of Colorado	USA	AMS
8	Contaminación Atmosférica, Departamento de Medio Ambiente, CIEMAT	ES	SMPS, CPC
9	Laboratory of Atmospheric Chemistry, PSI	CH	AMS
10	Jenoptic, Defense and Civil Systems	DE	Ceilometer
11	Wehrwissenschaftliches Institut für Schutztechnologien	DE	Ceilometer
12	Area de Medi Ambient, Diputació de Barcelona	ES	local support
13	Department of Physics-Physics of the Earth, University of Murcia	ES	modelling
14	Department of Chemistry, Carleton College	USA	Instrument support
15	Gencat	ES	Local support

Presenting SAPUSS

M. Dall'Osto et al.

Title Page

Abstract | Introduction

Conclusions | References

Tables | Figures

◄◄ | ►►

◄ | ►

Back | Close

Full Screen / Esc

Printer-friendly Version

Interactive Discussion

Table 2. Summary of measurements taken during SAPUSS.

Properties measured	Specific properties measured	Analytical technique	Temporal resolution	RS	UB	TM	TC (# = TCg)	RB
Meteorology	WD	Standard	1 h	V	V	V	V	V
	WS	Standard	1 h	V	V	V	V	V
	T	Standard	1 h	V	V	V	V	V
	RH	Standard	1 h	V	V	V	V	V
	Radiation	Standard	1 h	V	V	V	V	V
Remote sensing and boundary layer	Boundary layer	Radiosounding	12 h		V			
		Ceilometer CHM 15K	1 h		V (horizontal)		V# (vertical)	
Gaseous pollutants	CO	IR absorption	30 min	V	V		V#	V
	NO	Chemiluminescence	30 min	V	V		V#	V
	NO$_2$	Chemiluminescence	30 min	V	V		V#	V
	SO$_2$	UV fluorescence	30 min	V	V		V#	V
	O$_3$	UV absorption	30 min	V	V		V#	V
Aerosol mass loading		Impactor MOUDI	72	V				
		PM$_1$ Grav.	12	V	V			V
		PM$_{2.5}$ Grav.	24	V	V			
		PM$_{10}$ Grav.	12	V	V	V	V	V
		Grim	1 h	V	V	V	V, V# (both TC and Fabra)	V
Real time aerosol mass specrometry		AMS	10 min	V (HR-ToF-AMS)	V (HR-ToF-AMS)			
		ATOFMS	real time	V (TSI 3800-030)	V (TSI 3800-100)			
		PIXE	1 h	V				
Black Carbon		MAAP-Aethalometer	10 min	V (MAAP)	V (MAAP)	V (Magee AE-21 Aethalometer)	V (MAAP)	V (MAAP)
Particle number concentration	(> 3 nm)	CPC	1 m			V (TSI 3025)	V (TSI WB3786)	
	(> 5–7 nm)	CPC	1 m	V (TSI 3022)	V (TSI WB 3785)	V (TSI 3022)	V (TSI 3022)	V (TSI WB 3785)
Aerosol size resolved	15–600 nm	SMPS	5 min	V (TSI 3080 + CPC 3010)	V (TSI 3080 + CPC 3775)		V# (TSI 3034 CPC inbuilt)	V (EUSAAR.IFT with CPC 3772)
Chemical analyis	Metals	ICP-MS, ICP-AES	12/24 h	V	V	V	V	V
	EC-OC	Sunset	12/24 h	V	V	V	V	V
	Organic speciation	GC-MS	12/24 h	V	V	V	V	V
	Inorganic species	IC	12/24 h	V	V	V	V	V

Table 3. Classification of air mass origins during SAPUSS.

Calendar day	Day of week	Holiday day	AIR MASS TYPE				
			0 a.m.	6 a.m.	12 p.m.	6 p.m.	Day air mass
19 Sep 2010	Sunday	V	REG	REG	REG	REG	REGIONAL
20 Sep 2010	Monday		REG	REG	REG	REG	REGIONAL
21 Sep 2010	Tuesday		REG	REG	REG	REG	REGIONAL
22 Sep 2010	Wednesday		AS/NAF	AS/NAF	AS/NAF	AS/NAF	NAF
23 Sep 2010	Thursday		NAF	NAF	NAF	NAF	NAF
24 Sep 2010	Friday	V	REG	REG	REG	REG	Transition
25 Sep 2010	Saturday	V	AN	AN	AN	AN	ATLANTIC
26 Sep 2010	Sunday	V	AN	AN	AN	AN	ATLANTIC
27 Sep 2010	Monday		AN	AN	AN	AN	ATLANTIC
28 Sep 2010	Tuesday		AN	AN	AN	AN	ATLANTIC
29 Sep 2010	Wednesday		REG	REG	REG	REG	REGIONAL
30 Sep 2010	Thursday		REG	REG	REG	REG	REGIONAL
1 Oct 2010	Friday		REG	REG	REG	REG	REGIONAL
2 Oct 2010	Saturday	V	REG	REG	REG	REG	Transition
3 Oct 2010	Sunday	V	R/NAF	R/NAF	R/NAF	R/NAF	NAF
4 Oct 2010	Monday		R/NAF	AN	AN	AN	Transition
5 Oct 2010	Tuesday		AN	AN	AN	AN	ATLANTIC
6 Oct 2010	Wednesday		AN	REG	REG	REG	Transition
7 Oct 2010	Thursday		NAF	NAF	NAF	NAF	NAF
8 Oct 2010	Friday		NAF	NAF	NAF	NAF	NAF
9 Oct 2010	Saturday	V	NAF	NAF	NAF	NAF	NAF
10 Oct 2010	Sunday	V	NAF	NAF	MED	MED	Transition
11 Oct 2010	Monday	V	MED	EUR	EUR	EUR	Transition
12 Oct 2010	Tuesday	V	EUR	EUR	EUR	EUR	EUROPE
13 Oct 2010	Wednesday		EUR	EUR	REG	REG	Transition
14 Oct 2010	Thursday		REG	REG	REG	REG	REGIONAL
15 Oct 2010	Friday		REG	REG	REG	REG	REGIONAL
16 Oct 2010	Saturday	V	REG	REG	REG	REG	REGIONAL
17 Oct 2010	Sunday	V	REG	REG	AN	AN	REGIONAL
18 Oct 2010	Monday		AN	AN	AN	AN	ATLANTIC
19 Oct 2010	Tuesday		AN	AN	AN	AN	ATLANTIC

Table 4. Average gaseous concentrations at different sites during SAPUSS. (NA not available). (*) Average between TC (1.0 ± 0.4) and TCg (1.1 ± 0.4).

		Measurement sites				
		RS	UB	TCg	TM	RB
Gaseous poll. ($\mu g\,m^{-3}$)	NO	8.8 ± 12	5.2 ± 13	1.5 ± 1.6	NA	1.0 ± 0.2
	NO_2	37 ± 19	28 ± 21	15 ± 12	NA	3.8 ± 3.9
	NO_x	46 ± 20	33 ± 25	17 ± 13	NA	5 ± 4
	CO	0.4 ± 0.3	0.3 ± 0.2	0.3 ± 0.1	NA	0.2 ± 0.3
	SO_2	2.1 ± 2.3	0.3 ± 1.2	0.7 ± 2.4	NA	0.5 ± 0.6
	O_3	43 ± 21	58 ± 22	73 ± 16	NA	62 ± 19
	NH_3	3.1 ± 0.4	2.1 ± 0.5	1.0* ± 0.4	2.0 ± 0.6	0.5 ± 0.2

Table 5. Average total particle number (N) and Black Carbon (BC) concentrations during SAPUSS.

	Measurement sites				
	RS	UB	TC	TM	RB
N (cm^{-3})	12 890 ± 6300	10 490 ± 6400	5500 ± 3800	9590 ± 6300	2600 ± 1800
BC (µg m^{-3})	2990 ± 1700	1350 ± 1100	659 ± 450	1405 ± 1500	450 ± 350

Table 6. Average aerosol mass loadings during SAPUSS.

Monitoring site	PM_{10}	$PM_{2.5}$	PM_1	$PM_{2.5}/PM_{10}$	PM_1/PM_{10}	Availability (%)
			Grimm			
RS	30.7	18.6	16.3	0.61	0.53	100
UB	25.9	16.2	12.4	0.63	0.48	98
TM	24.8	17.7	14.7	0.71	0.59	88
TC	19.2	16.9	14.0	0.88	0.73	45
TCg	21.8	15.8	11.1	0.73	0.51	70
RB	20.0	10.9	10.4	0.54	0.52	100
			Gravimetric			
						$(PM_{10} - PM_{2.5} - PM_1)$
RS	31.2	17.9	16.4	0.57	0.52	92 / 92 / 92
UB	25.8	16.2	12.3	0.63	0.48	85 / 78 / 78
TM	24.1	–	–	–	–	92 / – / –
TC	–	–	–	–	–	–
TCg	19.2	–	–	–	–	90 / – / –
RB	22.3	10.9	9.9	0.49	0.45	48/ 67 / 42

Table 7. Correlation table of aerosol mass loadings during SAPUSS.

	TM PM$_{10}$	TM PM$_{2.5}$	TM PM$_1$	TC PM$_{10}$	TC PM$_{2.5}$	TC PM$_1$	TCg PM$_{10}$	TCg PM$_{2.5}$	TCg PM$_1$	RS PM$_{10}$	RS PM$_{2.5}$	RS PM$_1$	UB PM$_{10}$	UB PM$_{2.5}$	UB PM$_1$	RB PM$_{10}$	RB PM$_{2.5}$	RB PM$_1$
TM (PM$_{10}$)		0.75	0.60				0.50	0.55	0.55		0.35	0.40	0.50	0.50	0.50			0.35
TM PM$_{2.5}$)			0.95	0.50	0.40	0.40	0.70	0.85	0.85		0.60	0.70	0.65	0.80	0.80		0.35	0.40
TM PM$_1$)				0.40		0.40	0.65	0.85	0.85		0.55	0.75	0.55	0.75	0.85			0.40
TC (PM$_{10}$)					0.91	0.85	0.50	0.70	0.70		0.56	0.55	0.40	0.60	0.50			0.40
TC PM$_{2.5}$)						0.95	0.40	0.75	0.75		0.60	0.60		0.60	0.50		0.45	0.45
TC PM$_1$)							0.75	0.75			0.60	0.60		0.55	0.50		0.42	0.45
TCg (PM$_{10}$)								0.85	0.85		0.75	0.75	0.70	0.75	0.70		0.40	0.45
TCg PM$_{2.5}$)									0.95		0.80	0.85	0.70	0.85	0.90		0.40	0.50
TCg PM$_1$)											0.80	0.85	0.66	0.90	0.90		0.40	0.50
RS (PM$_{10}$)											0.60	0.50	0.55					
RS PM$_{2.5}$)												0.95	0.50	0.60	0.50			
RS PM$_1$)													0.45	0.60	0.60			
UB (PM$_{10}$)														0.80	0.70			
UB PM$_{2.5}$)															0.95			0.40
UB PM$_1$)																		0.40
RB (PM$_{10}$)																	0.80	0.65
RB PM$_{2.5}$)																		0.90
RB PM$_1$)																		

Title Page

Abstract | Introduction

Conclusions | References

Tables | Figures

|◄ | ►|

◄ | ►

Back | Close

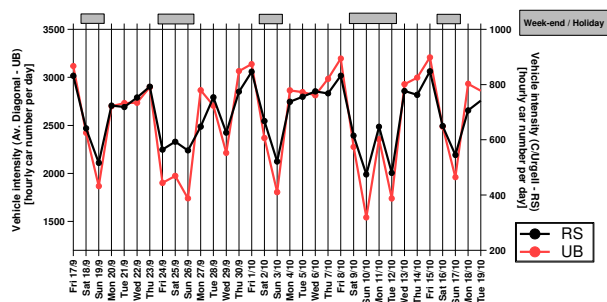Full Screen / Esc

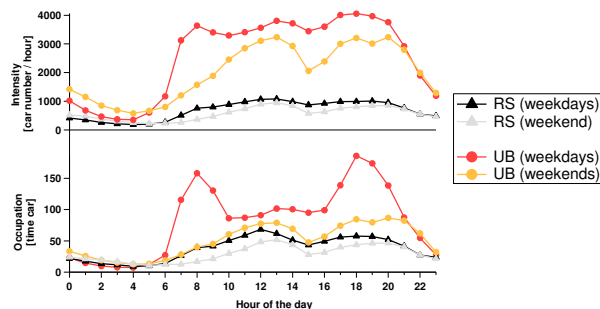Printer-friendly Version

Interactive Discussion

Table 8. Mean concentrations ($\mu g\,m^{-3}$) of 12 h resolution measurements from filters of OM, EC, SO_4^{2-}, NO_3^-, NH_4^+, crustal, marine, and unaccounted mass in PM_1, PM_{1-10} PM_{10} fractions at different SAPUSS monitoring sites (RS, UB, RB). Please note that only PM_{10} concentrations are available for the the TM and TCg site.

| | SAPUSS monitoring site | | | | | | | | | | |
| | RS | | | UB | | | RB | | | TM | TC |
	PM_1 (fine)	PM_{1-10} (coarse)	PM_{10} (tot.)	PM_1 (fine)	PM_{1-10} (coarse)	PM_{10} (tot.)	PM_1 (fine)	PM_{1-10} (coarse)	PM_{10} (tot.)	PM_{10} (tot.)	PM_{10} (tot.)
OC	3.5	0.13	3.7	2.1	0.44	2.5	1.7	1.3	3	2.5	2.2
EC	1.4	0.0	1.4	0.69	0.0	0.9	0.19	0.0	0.27	0.67	0.47
SO_4^{2-}	2	0.74	2.8	1.8	1.0	2.8	1.5	0.87	2.3	2.7	2.30
NO_3^-	0.64	1.9	2.6	0.46	1.7	2.2	0.15	1.4	1.5	2.4	1.6
$NH4^+$	0.78	0.12	0.9	0.61	0.09	0.7	0.46	0.16	0.63	0.69	0.50
Crustal	0.38	5.2	5.5	0.63	3.4	4.1	0.17	2.5	2.7	3.7	3.2
Marine	0.46	1.9	2.4	0.30	1.6	1.9	0.49	0.41	0.91	2.4	1.4
% Deter.	63.9	63.9	64.1	43	43	55.6	41.5	41.5	53.4	51.9	59.5

Table 9. Results of the evaluation of the modeling system applied during the SAPUSS field campaign versus observations: Observed Mean (OM); Model Mean (MM); Bias (B); Mean Normalized Bias (MNB); Observed Standard Deviation (OSD); Model Standard Deviation (MSD); Percentual Bias of the Standard Deviation (PBSD).

Monitoring site	OM ($\mu g\,m^{-3}$)	MM ($\mu g\,m^{-3}$)	B ($\mu g\,m^{-3}$)	MNB (%)	OSD ($\mu g\,m^{-3}$)	MSD ($\mu g\,m^{-3}$)	PBSD (%)
			PM_{10}				
RS	34.37	22.09	−12.28	−35.75	16.01	12.09	−24.47
TM	26.19	16.05	−10.14	−38.72	13.39	13.18	−1.60
UB	27.67	20.12	−7.55	−27.29	11.23	8.56	−23.78
TCg	21.43	18.78	−2.65	−12.39	8.77	9.58	9.35
TC	19.32	18.26	−1.05	−5.45	4.26	5.31	24.55
RB	19.80	10.34	−9.46	−47.79	11.44	7.56	−33.92
			$PM_{2.5}$				
RS	20.55	13.93	−6.62	−32.23	8.09	7.13	−11.81
TM	19.35	11.88	−7.47	−38.59	9.65	6.45	−33.13
UB	17.75	14.21	−3.54	−19.96	8.57	6.95	−18.88
TCg	16.61	12.62	−3.99	−24.03	8.16	5.12	−37.26
TC	17.40	13.02	−4.38	−25.19	4.01	4.99	24.56
RB	10.91	8.47	−2.44	−32.37	4.41	5.95	34.87
			PM_1				
RS	17.99	10.90	−7.09	−35.42	7.47	5.77	−22.73
TM	16.15	10.04	−6.11	−37.85	8.64	6.47	−25.11
UB	13.23	10.09	−3.14	−23.73	4.62	6.03	30.50
TCg	11.97	8.99	−2.98	−24.92	7.11	5.01	−29.51
TC	14.73	10.66	−4.07	−27.62	3.64	3.44	−5.57
RB	10.56	7.22	−3.34	−31.62	5.41	6.03	11.40
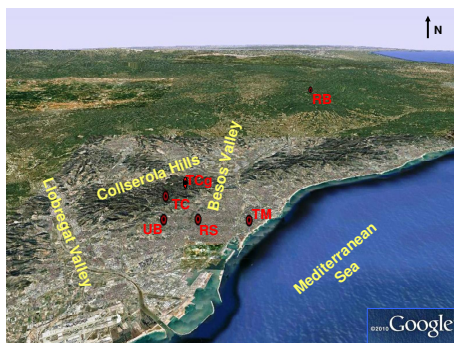
(a)

(b)

Fig. 1. Maps of measurement sites used in SAPUSS: Road site (RS), Urban Background (UB), Tower Mapfre (TM), Tower Callserola (TC), Fabra observatory (TCg) and Regional Montseny background site (RB).

(c)
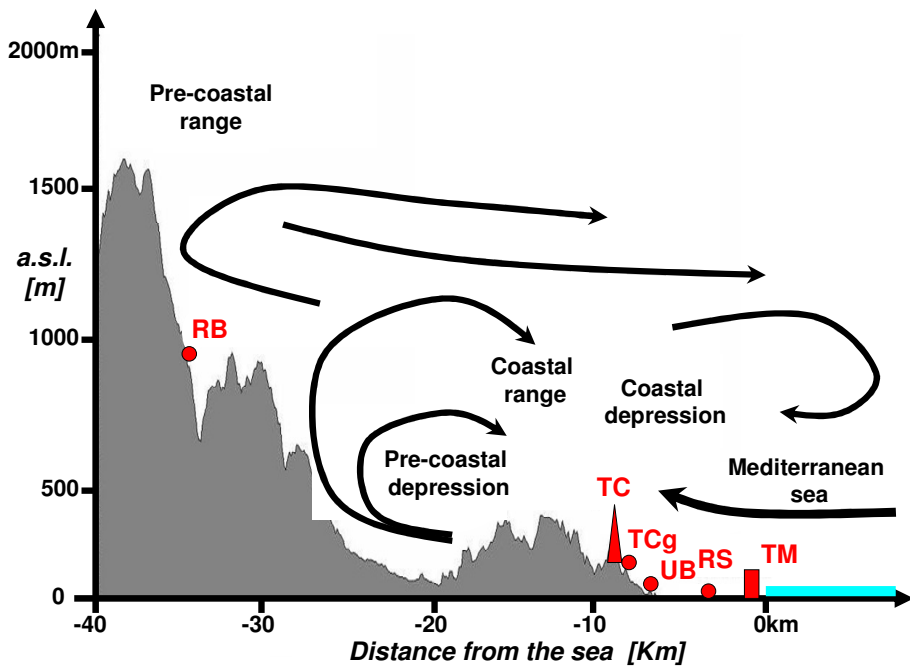
Fig. 1. Continued.

Fig. 2. (a) Average hourly number of vehicles per day at Road Urgell (road RS site) and at the Avenida Diagonal (close to the UB) and **(b)** diurnal traffic intensity and traffic occupation at the RS site and at the Avenida Diagonal (UB).
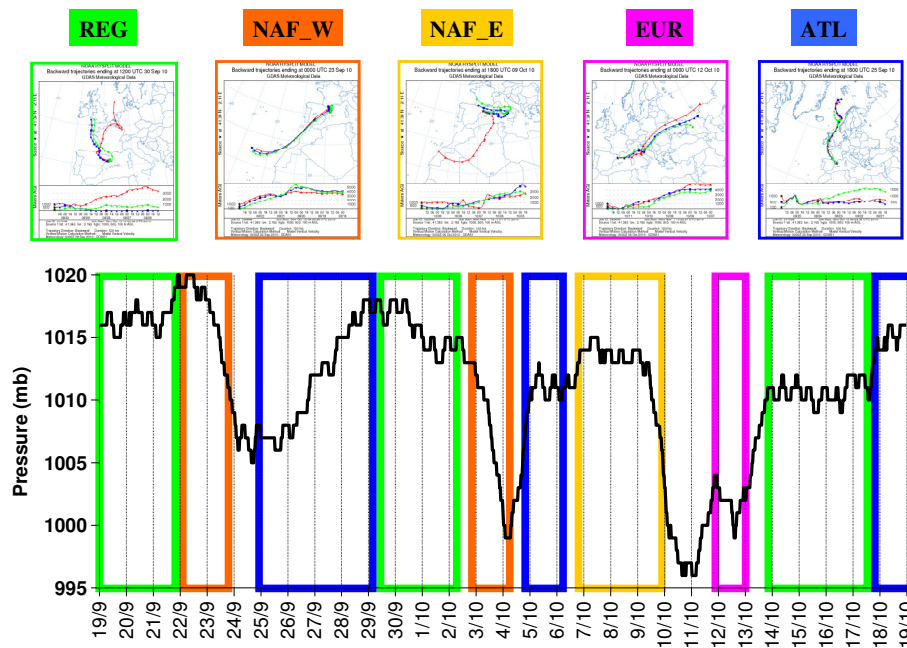
Fig. 3. Atmospheric pressure (mb) and temporal trend of air mass origins during SAPUSS.

Full Screen / Esc

Printer-friendly Version

Interactive Discussion
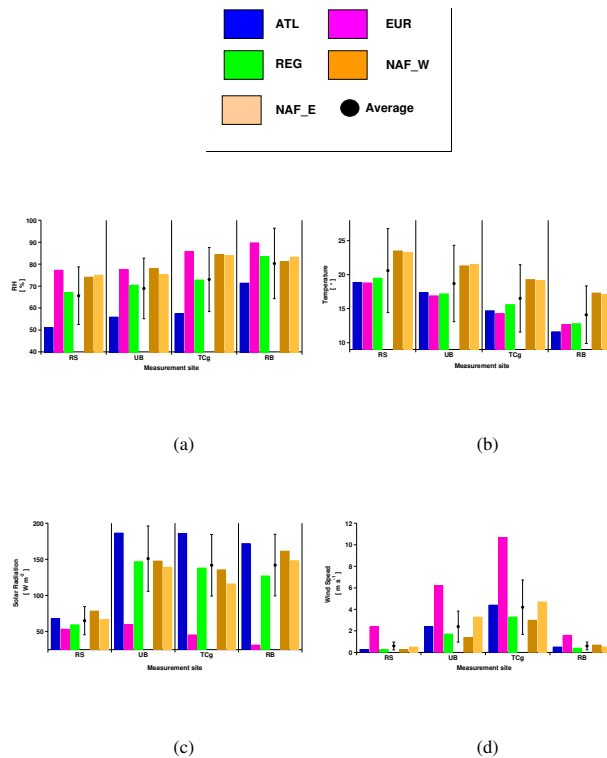
Fig. 4. Average **(a)** RH, **(b)** temperature, **(c)** solar radiation and **(d)** wind speed during SAPUSS for different air mass types at four different monitoring sites. Please note black dots show average values (±1σ).
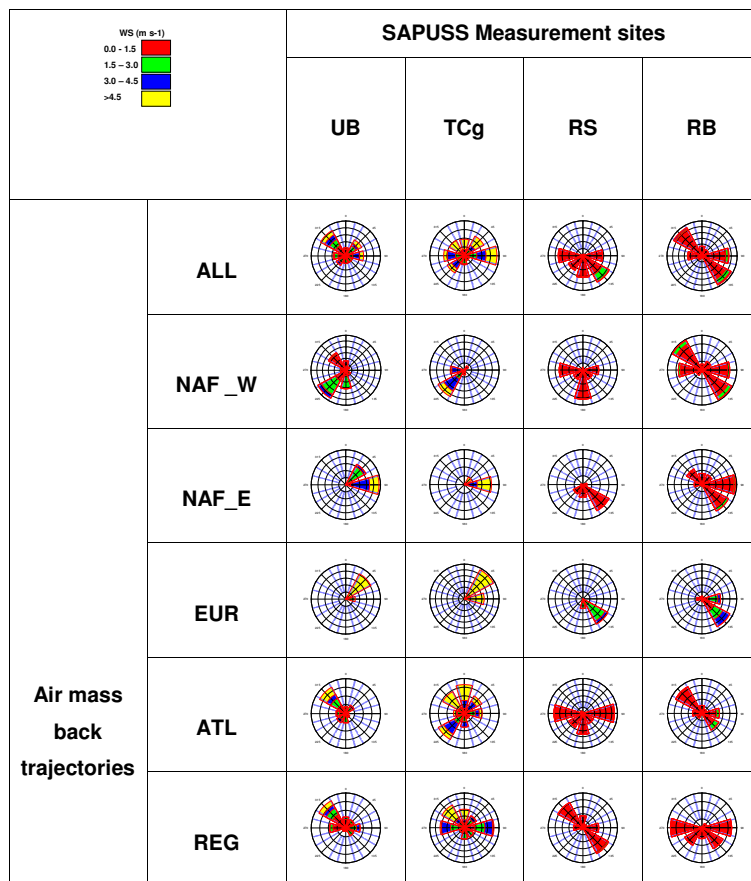
Fig. 5. Wind roses at four different SAPUSS monitoring sites for all study (ALL) and for selected air mass types.

Printer-friendly Version

Interactive Discussion
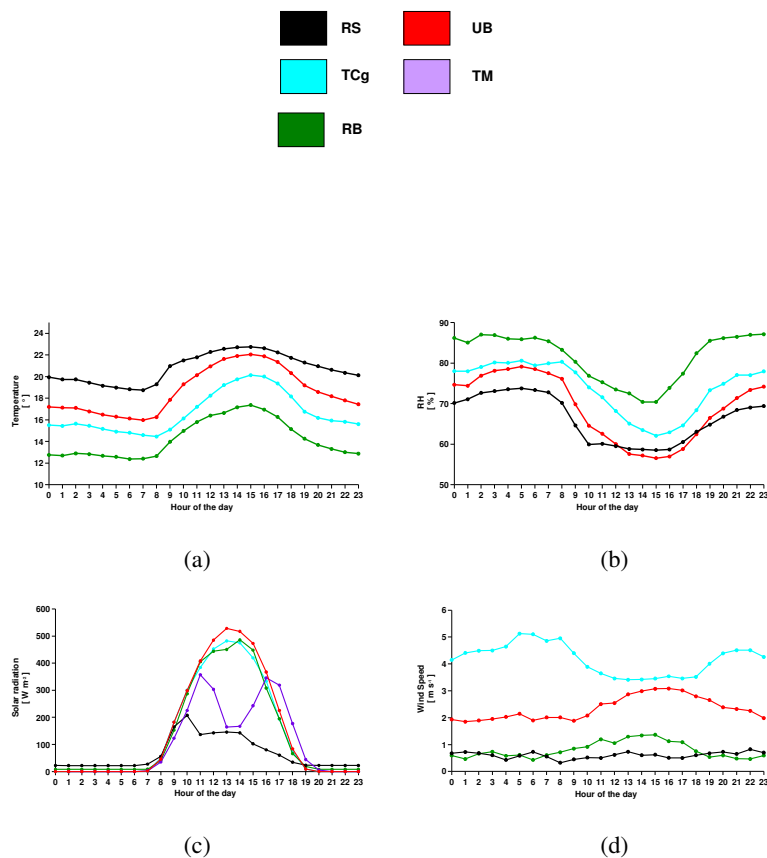
Fig. 6. Diurnal average Temperature **(a)**, RH **(b)**, Solar Radiation **(c)** and wind speed **(d)** at five different SAPUSS monitoring sites.

Scenario	Wind speed	Wind direction
(a) Atlantic (25th September 2010)		
(b) Europe (12th October 2010)		
(c) Regional (30th September 2010)		
(d) NAF_W (3rd October 2010)		
(e) NAF_E (9th October 2010)		

Legend: RS, UB, TCg, RB
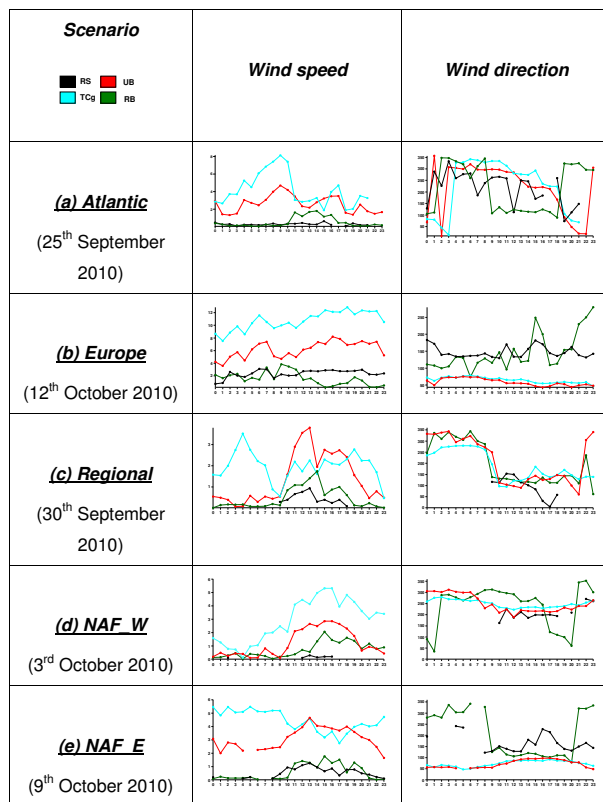
Fig. 7. Diurnal WS and WD average measurements at four SAPUSS monitoring sites under different air mass types.
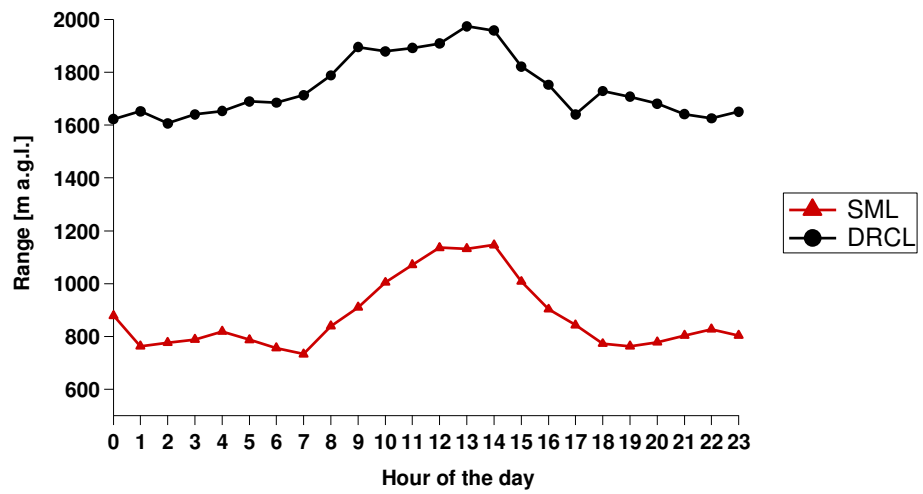
Fig. 8. Diurnal variation of the surface mixed layer (SML) and the decoupled residual or convective layer (DRCL) during SAPUSS.
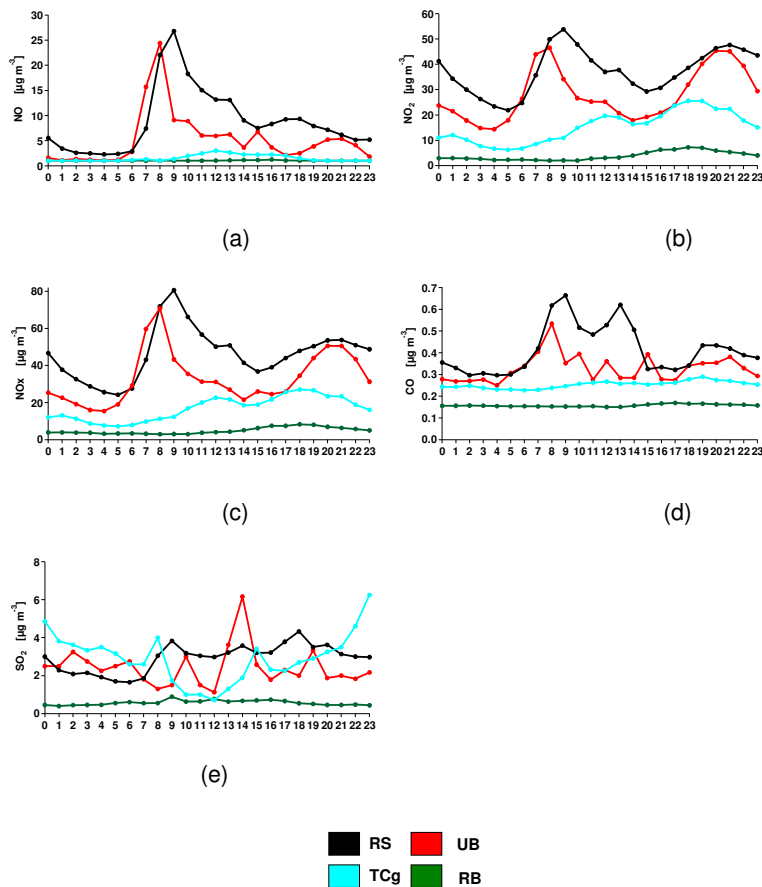
Fig. 9. Diurnal variation of gaseous measurements at four different monitoring sites **(a)** NO, **(b)** NO_2, **(c)** NO_x, **(d)** CO, **(e)** SO_2. Ozone is reported in Fig. 12a.

Full Screen / Esc
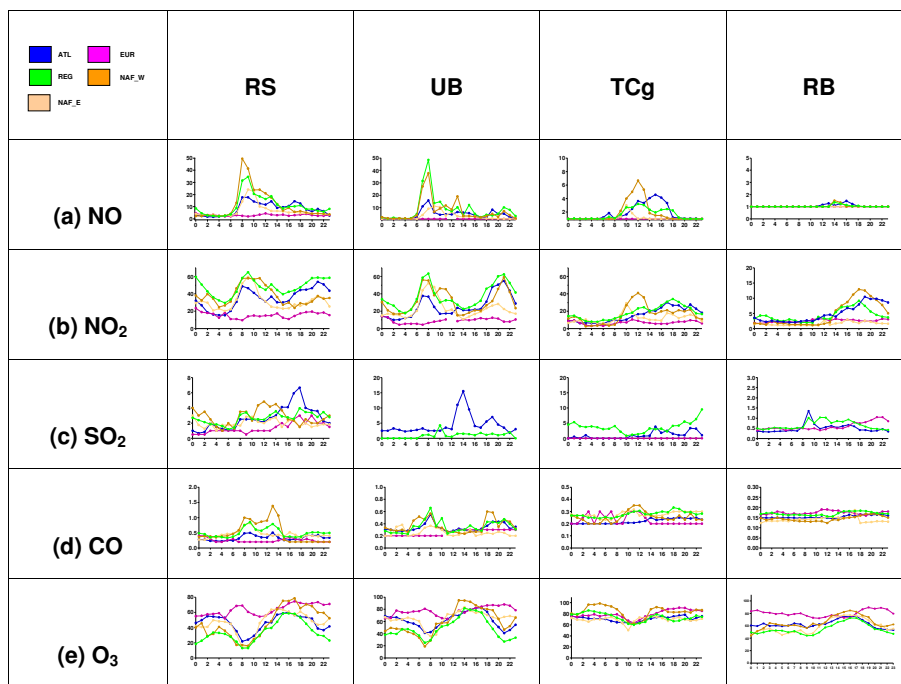
Fig. 10. Diurnal variation at four different monitoring sites for **(a)** NO, **(b)** NO_2, **(c)** SO_2, **(d)** CO, **(e)** O_3 for different air mass types. Please note all concentrations are in $\mu g\,m^{-3}$.
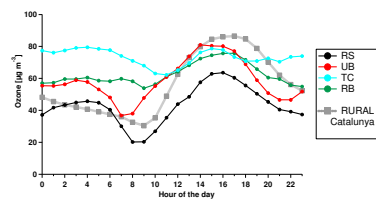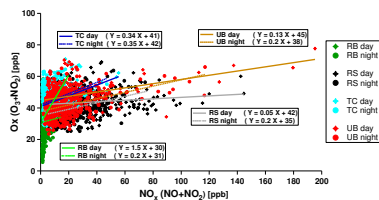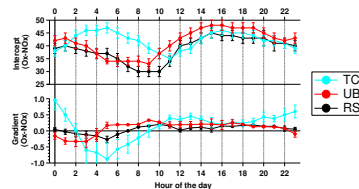
Fig. 11. (a) Diurnal variation of ozone concentrations at 4 SAPUSS monitoring sites (RS, UB, TC, RB) and at REGIONAL Catalunya (average of 7 monitoring station at regional sites in the province of Catalunya); **(b)** Oxidant Plot of the variation in volume mixing ratio of O_x ($NO_2 + O_3$) as a function of NO_x ($NO + NO_2$) for 4 SAPUSS sites. Data are for day (08:00–16:00) and night (20:00–08:00) hourly averages for the whole SAPUSS campaign period; **(c)** variation in the intercept and gradient of the regression analyses of oxidant plots (as shown in Fig. 12b), for each hour of the 24-h period averaged over the campaign duration.

Title Page

Abstract · Introduction

Conclusions · References

Tables · Figures

|◄ · ►|

◄ · ►

Back · Close

Full Screen / Esc

Printer-friendly Version

Interactive Discussion
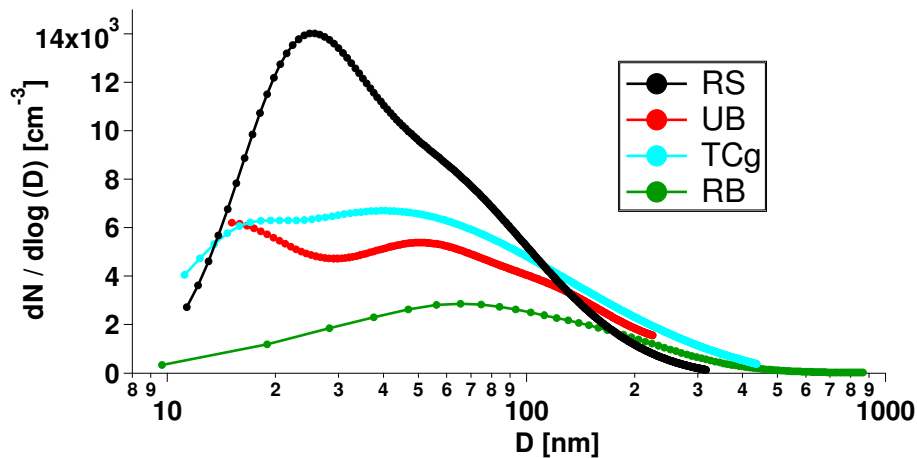
Fig. 12. SMPS aerosol size distribution obtained simultaneously at 4 monitoring sites for the whole period of SAPUSS.
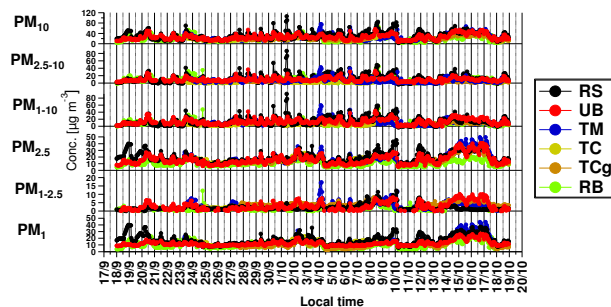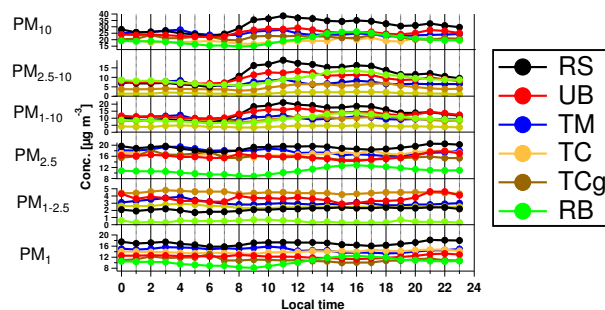
Fig. 13. Temporal trends **(a)** and diurnal variation of selected aerosol PM_x mass **(b)** for all the SAPUSS studies. **(c)** represents selected case study periods: Regional conditions (Reg.: stagnant regional air masses without accumulation of nitrate containing aerosols, 29–30 September 2010) and Regional conditions with nitrate (Reg-Nit: stagnant regional air masses with accumulation of nitrate containing aerosols, 15–16 October 2010).
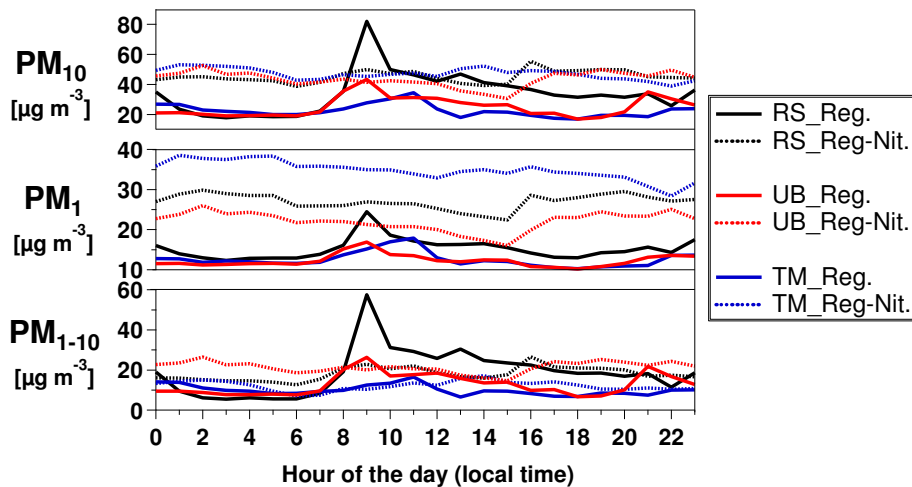
Fig. 13. Continued.
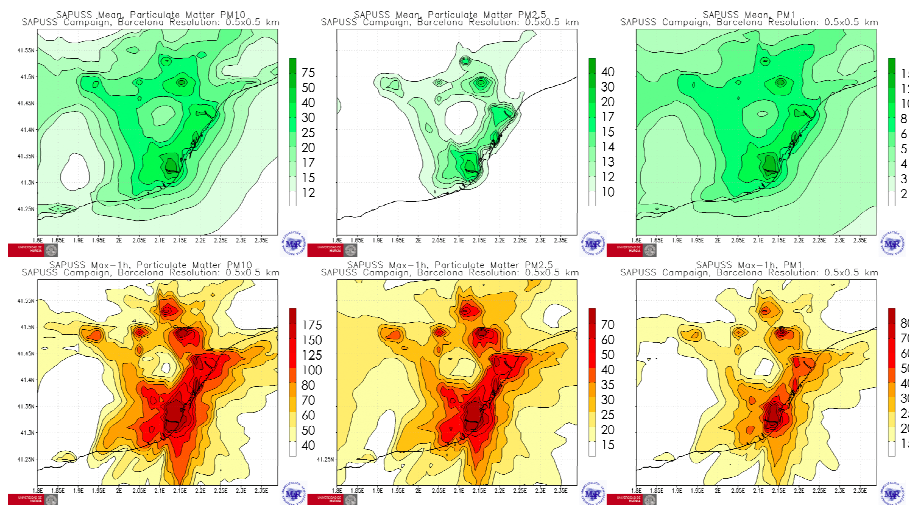
M. Dall'Osto et al.

Fig. 14. Mean (top row) and 1-h maximum (bottom row) ground-level concentrations of (from left-right) PM_{10}, $PM_{2.5}$ and PM_1 modeled during the SAPUSS field campaign in the Barcelona Metropolitan Area. Levels are expressed in $\mu g\,m^{-3}$.